Provenance of Early Pleistocene sediments based on a high-resolution sedimentological dataset of borehole Petten, southern North Sea

Hao Ding

6559972

A thesis submitted for the degree of

MSc Earth, Life and Climate

Utrecht University

Utrecht University

July, 2020

Preface and Acknowledgements

This thesis was written as part of the Master of Science degree in Earth Sciences, program Earth, Life and Climate, at Utrecht University. The research was performed under the supervision of Kim Cohen and Wim Hoek, also with help of Timme Donders and Alexander Houben. This research, together with a parallel research conducted by Lissane Krom, contributes to a larger project in paleoenvironment reconstruction of the Early Pleistocene in the southern North Sea Basin, based on the Petten Borehole 1. This thesis focused on sedimentology, and the parallel thesis by Krom focused on palynology.

For the process of this project, I would like to express my gratitude to my supervisors Kim Cohen and Wim Hoek for their great effort on the research and lab work guidance. All the redactional and scientific comments on my writing from Kim Cohen are highly appreciated. I would also like to thank Timme Donders, Alexander Houben and Lisanne Krom for all the cross-disciplinary discussions as well as the assistance on my final presentation. Last but not least, I would like to thank my family and friends, who have been supporting me as always during this Covid-19 pandemic. Studying abroad has been tough, but I really appreciate all the love and encouragement around me, no matter how far apart we are.

Abstract

In 2018, a fairly complete core (Petten BH 1) reaching over 300 meters into the unconsolidated, dominantly sandy Pleistocene sequence was recovered in the northwest of the Netherlands, in the coastal dune area along the present North Sea. The good recovery of the interval below 200 m depth allows combined sedimentological and palynological study in the same core. Therefore, we conducted two parallel studies of sedimentology (this MSc thesis) and palynology (MSc thesis by Krom) in the interval 200 – 380 m of the Petten BH 1, which is believed to cover the Early Pleistocene sequence in the southern North Sea Basin.

In this study, we aimed to 1) reconstruct the sedimentary environment, 2) investigate the provenance of the sediments, and 3) find out the reworking and hiatus in the sedimentary history. We have used lithological-sedimentological logging, grain size analysis, heavy mineral analysis and element concentrations measurement to conduct the research. The results reveal a shallowing upwards water depth trend, with superimposed glacial-interglacial sea-level cycles, which makes that the core can be divided into three intervals, the marine/pro-deltaic phase (330 – 380 m), littoral/deltaic front phase (270 – 330 m), and fluvial/delta plain phase (200 – 270 m). As the analysis of heavy mineral composition is still in progress, the provenance of sediments has not yet been convincingly identified. However, the good correlations between heavy mineral weight percent and Zr, Ti are supporting evidences of considerable components of easterly source (Eridanos). Erosion events occurred frequently from 330 m upwards, due to sea level change and river response to this (low stand incision, transgressive reworking, high stand avulsion; repeatedly). Some erosion events are clearly recognized as sediment contacts, while other erosion events, including major erosion events in the fluvial sediment, are in the intervals that were not recovered. These findings also held up when they were integrated with the palynological study, strengthening our sedimentary environmental conclusions.

Contents

1. Introduction

1.1 Research Subject

The North Sea Basin has been a depocenter in northwestern Europe since Cenozoic (Huuse et al., 2001; Kuhlmann et al., 2004), and the Pleistocene deposits in the basin formed most part of the Netherlands and its adjacent area (Gibbard et al., 1988; Westerhoff, 2009; Cohen et al., 2014). The characteristic glaciation cycles starting from the end of Pliocene (e.g. Lisiecki and Raymo, 2007; Ruddiman, 2014), together with the Pleistocene tectonic subsidence of the North Sea Basin (e.g. Kooi et al., 1991) and development of a huge delta complex (e.g. Gibbard et al., 1988), have resulted in a complicated sedimentary environment and tremendous thickness of the Quaternary deposits in the basin (Gibbard et al., 1988; Kooi et al., 1991; Donders et al., 2018). A wealth of research output exists to reconstruct the Pleistocene paleoclimate and the sedimentary history in the North Sea Basin, as well as the stratigraphic correlations among inland, onshore and offshore records.

Westerhoff (2009) in the introduction of his PhD thesis, stated that the Late Pliocene and the Early Pleistocene deposits from outcrops and boreholes along the southern rim of the North Sea Basin (i.e. the southern part of the Netherlands) have been long investigated, both in paleontology and sediment-petrography. Hence a paleontologically based stratigraphic framework for the Late Cenozoic was made over 100 years ago, which in the second half of the 20th century was further divided into stages and substages considering palynology. Historically, the stratigraphic correlations and geological mapping relied strongly on being able to sample and correctly identify these pollen associations, as well as on the results from heavy mineral investigations (Westerhoff, 2009). This does not work so well, however, away from the edges of the basin towards the depocenter areas in coastal and shelf-sea marine environments, such as in the northern Netherlands and the Dutch sector of the North Sea. This also made the linkage of the land-based (chrono)stratigraphy of the southern Netherlands with the marine realm and its biostratigraphy and also Marine Isotope Stages (MIS) less accurate. Investigations and reconstructions performed on onshore and offshore cores may overcome the correlation-accuracy problems, and researchers also worked on that in the last few years. Recently, Noorbergen et al. (2015) and Donders et al. (2018) have used organic geochemical and palynological data to narrow down the timeframe and establish linkage to MIS, respectively using

the onshore core and the offshore core. In addition, research on provenance of sediments (Kuhlmann et al., 2004) and fluvial/deltaic evolution (Gibbard et al., 1988; Overeem et al., 2001) in the southern North Sea also provided information to build or revise the stratigraphic framework.

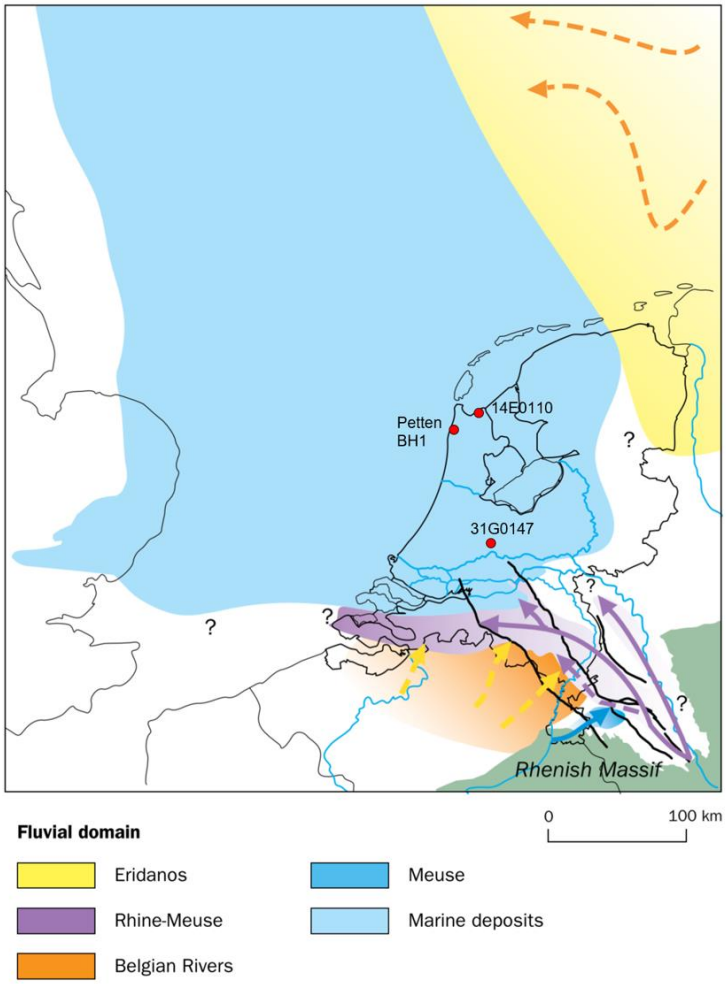

Figure 1 *Situation map of the southern North Sea Basin at the beginning of Pleistocene, with fluvial domains and estimated coast line position (after Westerhoff, 2009: Figure 6.9B). The locations of Petten Borehole 1 and other boreholes mentioned in the text are indicated.*

In 2018, two fairly complete cores reaching over 300 meters into the unconsolidated, dominantly sandy Pleistocene sequence were recovered in the northwest of the Netherlands (Petten), in the coastal dune area along the present North Sea (**Figure 1**). They were transferred to TNO Geological Survey of the Netherlands

for description and research. The pair of cores were located on either side of a northwest-southeast fault recognized on seismic profiles. Their initial results would be integrated to develop a seismic risk-assessment. In a larger view, the cores recovered materials from an important location in the Quaternary depocenter in the southern North Sea Basin. They sampled an area known to have experienced the complicated deltaic evolution and landscape change during the Early Pleistocene (Gibbard et al., 1988; Westerhoff, 2009; Cohen et al., 2014). Also, the good recovery of the lower half of Borehole 1 allowed combined sedimentary and palynological study, which is critical to build an independent chronostratigraphy and link the inland fluvial records to their depocenter shallow marine equivalents better. Hence TNO in cooperation with Utrecht University aimed to perform detailed research on the lower half of Petten Borehole 1.

1.2 Aim of the Project

The MSc project resulting in this thesis, made use of the lower half of Petten Borehole 1 and focused on generating high-resolution sedimentological and marine and terrestrial palynological datasets. In general, the aim of the project is to construct a new reference section for the Pleistocene of the shallow marine to deltaic facies of the Netherlands, and to reconstruct the regional response to glacio-eustatic and paleoclimatic change. Therefore, the overall project consists of two student sub-projects in 2019-2020, performed in this thesis (Ding: sedimentology) and a parallel thesis (Krom: palynology). TNO and Utrecht University researchers had also worked on the cores in 2018-2019 (Houben, 2019: palynology, paleomagnetism). Particularly, this thesis aims to investigate the following:

a) The sedimentary environment. The Quaternary glaciation-interglaciation cycles had major impact on the global and regional environment change, and the change was recorded in the deposits. By building a high-resolution sedimentological and lithological loggings, we can reconstruct trends and sequences in the water depth and in indications for past conditions of water flow (high energy channel sands, lower energy tidal flats and under water muds), and the regional response to the sea-level change. Element concentration and grain size distribution can also help these aspects of the reconstruction.

b) The provenance of the sediments. Heavy mineral analysis has been used to deduce the source regions of the sediment, by recognizing different heavy mineral associations. With this information, we can learn better about the evolution of the

Eridanos and Rhine-Meuse river systems, as well as the relative timing of major spatial shifts in these systems.

c) Reworking and hiatus in the sedimentary history. Hijma et al. (2012) reviewed that the southern North Sea Basin experienced progressive reworking and net erosion in the Early and Middle Pleistocene. This thesis attempts to pinpoint the reworking and erosion events in the Petten Borehole 1 core.

The parallel thesis (Krom, 2020) aimed to produce high-resolution palynological and paleontological datasets with pollen and dinocyst records. It provides observations on paleoenvironmental change, alternation of terrestrial and marine realm, and reworking events. By discovering the first and/or last occurrence of certain species, and having cross-checks on sedimentary continuity, more accurate constraints for the age model of the core are produced (especially when the results of the thesis subprojects and that of prior work by TNO and UU workers are all combined). A final goal in this study was to cross-verify and integrate our sedimentary results with the findings from the palynological study, so that sedimentary environmental and chronostratigraphic conclusions are stronger.

1.3 Outline of the Thesis

The following part of the thesis will be started from Background (Chapter 2), where the geological setting, climate variability and the specific deltaic deposits will be introduced. Chapter 3 is about the Materials and Methods, showing the main works and analyses done in this thesis (sedimentological-lithological logging, grain size analysis, heavy mineral analysis, and XRF measurement). Also, the prior work done at TNO and the methods used in the parallel palynological thesis will be mentioned. Chapter 4 is the Results, which will be developed in accordance with the subsections in Chapter 3. Chapter 5 is the Interpretation in regard to provenance, sea-level change and erosion events. Chapter 6 is the Discussion, where the results and evidences found in this thesis will be discussed altogether. With the findings from the palynological study, integrated sedimentary indications and conclusions are also discussed in Chapter 5 and 6. Then the last section is the Conclusion (Section 7).

2. Background

2.1 Geological Setting

The epicontinental North Sea area in a tectonic sense was dominated by two east-west trending basins during Cretaceous (Glennie and Underhill, 1998) that developed into the North Sea Basin starting in the Early Cenozoic (Huuse et al., 2001). By the time of the Neogene, the North Sea Basin was confined by Fennoscandian landmass to the northeast, Mainland Europe to the southeast and the British Isles to the west, only with an opening towards the northwest to the Atlantic (Huuse et al., 2001; Donders et al., 2018). In the Quaternary, the tectonics of the North Sea Basin is mainly characterized by intermittent uplift of the rim which started from Pliocene (Kooi et al., 1998), and steady, long-term and relatively rapid subsidence of the basin (Kooi et al., 1991; Cohen et al., 2014). Subsidence rates of the North Sea Basin appear to have increased more than an order of magnitude from Paleogene and Neogene to Quaternary, which is attributed to the development of an intraplate stress field in Northwest Europe or regional flexural downwarping of the lithosphere in the Central Graben (Kooi et al., 1991). The high subsidence rate of the North Sea Basin, especially in the southern North Sea Basin, helped build the large thickness of the Quaternary deposition. With estimated 3500 m of Cenozoic sediment in some parts of the basin, Quaternary alone takes up over 1000 m in depocentres offshore (Gibbard et al., 1988; Kooi et al., 1991; Donders et al., 2018), comparing to the 380-m-deep Petten Borehole 1 with the age of the base Early Pleistocene. Besides the major tectonic activities, glacio- and hydro-isostasy, consistent with glaciation cycles in Quaternary, also modified the regional topography and landscapes in and around the North Sea Basin (Cohen et al., 2014).

Fluvial sediment in a terrestrial low-land environment was the dominant type of deposition in the North Sea Basin in Pleistocene, with occasional coastal, marine, glaciogenic or other types of deposition that were formed by glaciation and marine transgression (Hijma et al., 2012; Cohen et al., 2014). At the onset of Pleistocene, the coast line of the southern North Sea was further inland than present, with most of the Netherlands inundated during sea-level high stands (e.g. Westerhoff, 2009; **Figure 1**). Four main river systems played the major role feeding the southern North Sea Basin (Gibbard et al., 1988; Westerhoff, 2009). Three of these systems drained from the southern domain, which are Rhine, Meuse and Belgian rivers. The river systems from

the south can be regarded as one large river system, because they have once joined to another river system as tributaries in their complex evolving history (Gibbard et al., 1988). Rhine system is the longest of the northwest European drainage system, which currently has a drainage area of 185,000 km^2 (Busschers et al., 2007). The other river system is the Eridanos river system from the northeast, which was originated from Baltic region and has been feeding the North Sea basin since the Middle Neogene (Westerhoff, 2009). The river system is no longer existing as it gave way to glacial erosion in the Middle Pleistocene (Gibbard et al., 1988; Schüttenhelm and Laban, 2005; Overeem et al., 2001), since then leaving the smaller Rhine-Meuse system and central German rivers to supply the southern North Sea Basin. In the Neogene and in the Early Pleistocene, however, the Eridanos system played a big role in supplying fluvial sediment, judged by the volumes of its sediment in the first place – but also as the drainage area estimated to be 1.1×10^6 km^2 is considerable (Overeem et al., 2001), which is an order of magnitude larger than that of Rhine since the Early Pleistocene (present size: 1.85×10^5 km^2; Busschers et al., 2007). The evolving history and the deltaic deposits of Rhine-Meuse system and Eridanos system will be discussed later in this chapter.

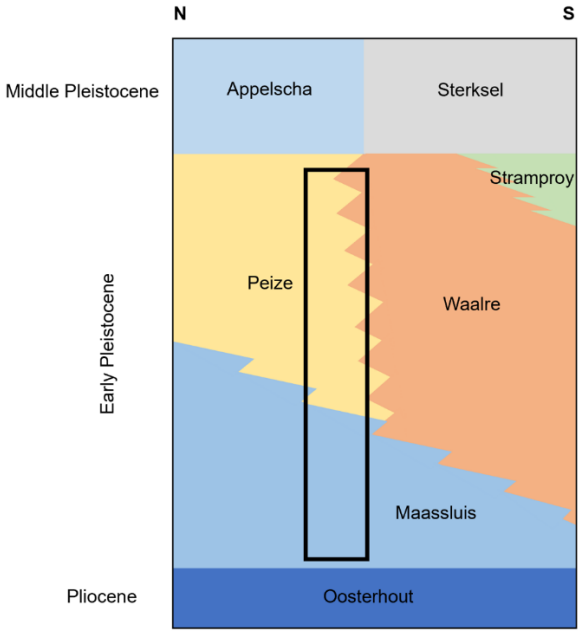

Figure 2 *Simplified Early Pleistocene lithostratigraphical units in the Netherlands, summarized based on Rijsdijk et al. (2005) and Westerhoff (2009). The black box shows the estimated location and interval of the Petten Borehole 1 that is studied in this thesis.*

The borehole site of this research is located nowadays onshore in the Holocene coastal plain of the northwest Netherlands. This part of the Netherlands was within the depocenter of the southern North Sea Basin since Neogene (e.g. Overeem et al., 2001; Westerhoff, 2009). The area has experienced severe change of landscape and deposition setting in the Early Pleistocene, and several sedimentary formations are identified (**Figure 2**). Oosterhout Formation and Maassluis Formation are defined as the depositions formed in shallow marine environments (Westerhoff, 2009), and attributed Late Pliocene and Early Pleistocene ages respectively. Then the river systems from east and south created a developing delta complex, and the fluvial deposits joined. As the Eridanos system gradually developed westwards, fluvial deposits were brought and made the Peize Formation (Westerhoff, 2009). Waalre Formation (including three subunits) was built by Rhine-Meuse system from the south, and Stramproy Formation by Belgian rivers in the further south (Westerhoff, 2009). After the termination of Eridanos system, Western German and Bohemian rivers, together with ice sheet drainage, continued to drain the area and built Appelscha Formation, while Rhine-Meuse extended northwards and built Sterksel Formation, mainly in the South and West of the Netherlands and adjacent North Sea (Rijsdijk et al., 2005; Westerhoff 2009). Then the composition of Rhine sediments changed markedly and is then known as the Urk Formation, the fluvial deposit from Rhine-Meuse system in the Middle Pleistocene, mainly in the east and north of the Netherlands and adjacent North Sea (Rijsdijk et al., 2005; Busschers et al., 2008). As the base of the Petten Borehole 1 is identified to be deposited during the Early Pleistocene, we can expect Maassluis Formation, Peize Formation and Waalre Formation, or maybe their interdigitations, in the lower half of the core.

2.2 Climate Variability in the Early Pleistocene (2.6 to 0.8 Ma)

The Pleistocene is known for its Northern Hemisphere glaciation cycles. The onset of the Northern Hemisphere glaciation happened approximately 2.7 Ma before present, and the size of ice sheets started to increase over each glaciation cycle from then on (Lisiecki and Raymo, 2007). In general, the Pleistocene is marked by a cold period which was gradually getting colder throughout the period. These are proved by the appearance of large amounts of ice-rafted debris in the North Atlantic and positive trending on North Atlantic benthic $\delta^{18}O$ data over the last 3 million years (e.g. Lisiecki and Raymo, 2005). The isotopic data also reveal that since 2.75 Ma the ice sheets

started to grow and melt at a cycle of 41,000 years, which was associated with the obliquity cycle. However, the character of the glaciation cycles began to change from 1.2 Ma, and it obviously became to a 100,000-year cycle after 0.5 Ma (e.g. Head and Gibbard, 2005; 2015). The longer glaciation cycles appeared together with larger ice sheets, severer extension of glaciation, longer glacial intervals, larger amplitude of glacial-interglacial cycles and a colder world. Lisiecki and Raymo (2007) also proposed that the duration of interglacial periods has decreased since the Early Pleistocene transition at 1.4 Ma. To summarize, the Early Pleistocene brought in the characteristic glaciation cycles and a cooling world, but not yet stepped into the period with stronger ice ages.

Some division methods are used to provide a more intuitive context to discuss the climate variability in the Early Pleistocene (**Figure 3**). Marine Isotope Stages (MIS) are the standard subdivisions of benthic $\delta^{18}O$ record, of which interglacial periods are given odd numbers and glacial periods even numbers. The first cold phase of Pleistocene was assigned with MIS 102, and the Early Pleistocene ranges from MIS 102 to MIS 20. Another division method is applied by distinguishing relative colder and warmer stages in a larger scale than MIS. The stages are determined distinctively in different regions. As in the Northwest Europe, the Early Pleistocene went through Praetiglian (cold), Tiglian (warm), Eburonian (cold), Waalian (warm), Menapian (cold), Bavelian (warm) (Zagwijn, 1985), and then went into Cromerian Complex, the Middle Pleistocene.

2.3 The Deltaic Deposits of the Eridanos and the Rhine-Meuse River Systems

As mentioned above, the large mass of the Early Pleistocene deposits in the southern North Sea Basin is attributed to the huge delta complex fed by several river systems (Eridanos, North German Rivers, Rhine, Thames, Meuse and Belgian Rivers; Gibbard et al., 1988). In terms of the study area of this research, the northwestern Netherlands, the Eridanos and the Rhine-Meuse river systems were mainly responsible (Rijsdijk et al., 2005; Westerhoff, 2009).

Due to the uplift of the Fennoscandian Shield since the Oligocene, the Eridanos river system had started to develop in the Baltic region. The drainage basin of the Eridanos system established during Late Oligocene or Early Miocene times, and the depocenters started to move westwards through the northwestern Europe since then (Overeem et al., 2001). In the Late Miocene, a straight longitudinal delta front was

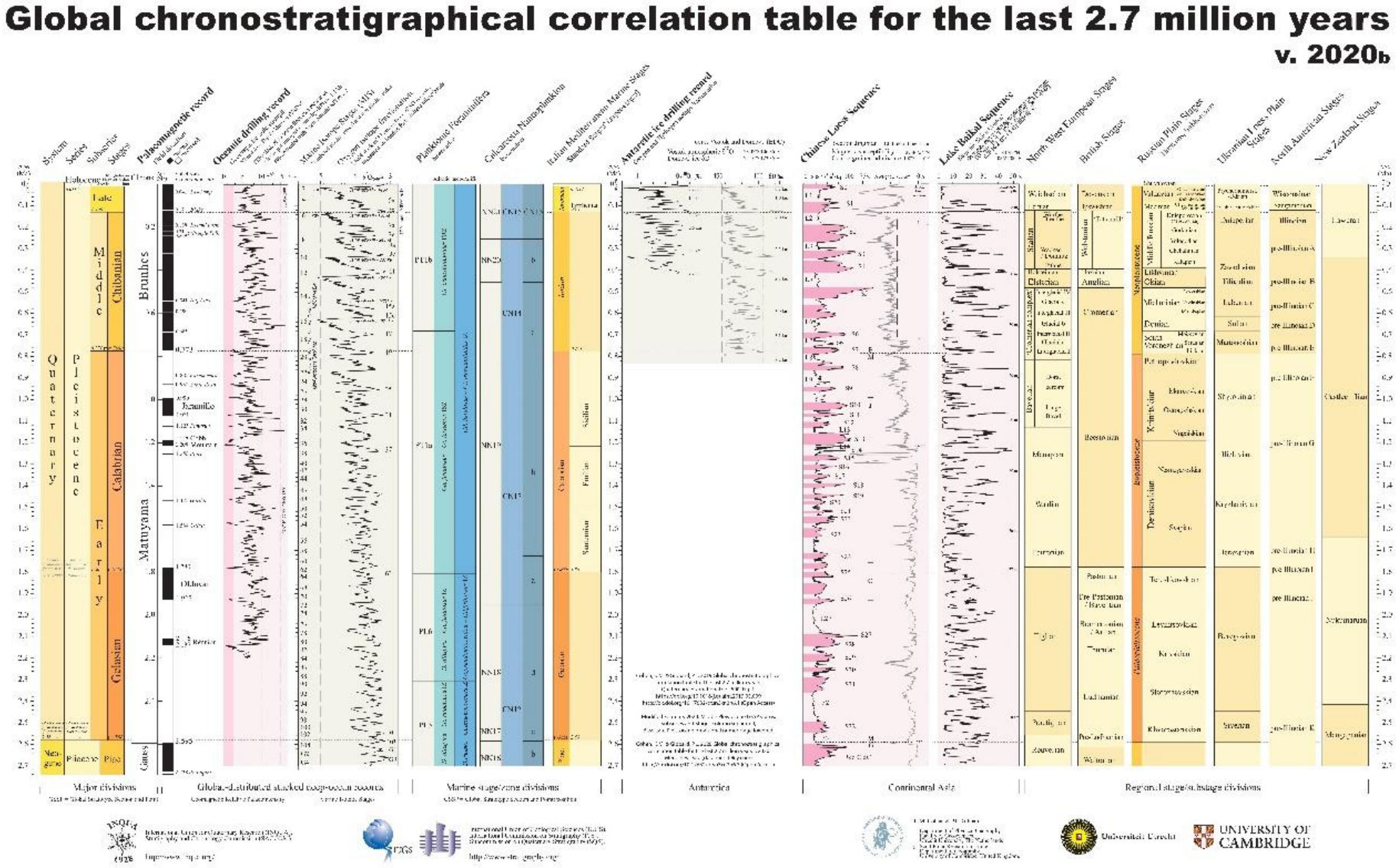

Figure 3 *Global chronostratigraphical correlation table for the last 2.7 million years, acquired from Cohen and Gibbard (2019).*

located in the east of the North Sea Basin (Danish and German sectors), and in the Early Pliocene, the deltaic area had a lobate front, with a developed distributary system. During the Late Pliocene, the distributary system repeatedly avulsed and erosively re-established parts of the channel network (Overeem et al., 2001). The depocenter had a southwards migrating trend in the Pliocene, and was located over the Central Graben right before the Pleistocene. It has been stated that braided rivers started to develop and build up the Peize Formation in the Netherlands during the Tiglian Stage (Overeem et al., 2001). The volumes of sediments represented by the Peize formation indicate a continuing expansion of the Eridanos system to the southwest. The rivers covered most of the country in the Waalian Stage, and this was also the time when Rhine-Meuse river system met the Eridanos in the central part of the Netherlands (Zagwijn, 1985; Gibbard et al., 1988; Overeem et al., 2001; Kuhlmann et al., 2004; Westerhoff, 2009).

Both the Rhine and the Meuse were formed in the Miocene, and the Rhine considerably enlarged its drainage basin by the end of Pliocene (Gibbard et al., 1988; Westerhoff, 2009). These two rivers joined together close to their entry point into the North Sea, to form the so-called Rhine-Meuse river system, which kept draining downstream to develop the deltaic area. In general, the deltaic area migrated northwards and westwards in the Late Pliocene and the Early Pleistocene. During the Late Pliocene, the progradation of the deltaic system increased rapidly (Kooi et al., 1991). It started to form the subunit WA-1 of the Waalre Formation in the Lower Rhine Embayment (LRE), to the southeast of the Netherlands and adjacent parts of Germany (Westerhoff, 2009), while the other part of the Netherlands (including the Petten locality) was mostly still inundated, forming the Oosterhout Formation. At the onset of the Pleistocene, the delta plain was located over the Roer Valley Graben (RVG), and built thick deposits of the subunit WA-2 of the Waalre Formation in the northern RVG (Westerhoff, 2009). WA-2 experienced the interdigitation with the deposits of Belgian rivers (Stramproy Formation) from the south and marine deposits (Maassluis Formation) from the north. Muds in the Maassluis Formation can be seen as pro-deltaic units of the Rhine delta system that produced the Waalre Formation, and of the Eridanos delta system that produced the Peize Formation. The impacts of Belgian rivers and marine deposits cut off the deposition of WA-2 by covering on top of it, which also acted as a boundary with the overlying subunit WA-3 of the Waalre Formation (Westerhoff, 2009). The deposition area of WA-3, including extensive flood-basins

(trapping muds), continued the extension northwards and westwards during the Early Pleistocene, and started interfingering and mixing with the Eridanos deposits (Peize Formation) in the central part of the Netherlands (Westerhoff, 2009). As the Rhine-Meuse river system kept extending northwestwards into former Eridanos deposition realm in the central Netherlands (Gibbard et al., 1988; Schüttenhelm and Laban, 2005; Overeem et al., 2001), it left former Rhine realms in the southern and western part of the country, in turn letting Belgian river system develop considerably (Stramproy Formation; Westerhoff, 2009). By the end of the Early Pleistocene, the southern North Sea Basin had evolved into a delta plain lowland fed by several river systems (Westerhoff, 2009).

Few lithological and petrographical features can help distinguish and characterize each Early Pleistocene formation in the southern North Sea Basin. Westerhoff (2009) summarized that the Maassluis Formation in the northern part of RVG contains medium to coarse sand, showing a coarsening-up trend in the lower part and a fining-up trend in the upper part. Clay layers also occur alternatively. This formation thickens to the north and northwest. The heavy mineral associations of the Maassluis Formation in the northern RVG are dominantly unstable, associated with garnet, epidote, saussurite/alterite and hornblende, which corresponds to the unstable heavy mineral associations from the Rhine. However, the unstable associations are not necessary to prominently exist further seawards to the north and northwest, where most of the Rhine depositions could not reach. Only the subunits WA-2 and WA-3 of the Waalre Formation were formed in the Early Pleistocene, which share similar lithology and architecture. The onset of the cold Pre-Tiglian Stage made a marked change of the depositional style with input of gravel and sand which was stripped off from the deep regolith formed in the Pliocene (Gibbard et al., 1988). Each subunit contains a number of stacked coarse grain (gravel/sand) to fine grain (clay) cycles, and peat layers can be found within clay deposits. The Waalre Formation has an unstable heavy mineral association, as it was fed by the Rhine river system. In contrast, the Peize Formation, formed by the Eridanos river system, has a stable heavy mineral association, characterized by garnet, epidote, hornblende, staurolite, metamorphic minerals and tourmaline (Westerhoff, 2009).

Westerhoff (2009) reviewed several boreholes in the Netherlands to discuss the correlations of the Quaternary sediments in the southern North Sea Basin, including the Borehole De Meern (31G0147) from the central Netherlands and the Borehole

Hipolytushoef (14E0110) from the northwest Netherlands (**Figure 1**). One of the differences in their lithological loggings is the overlying formations on the Maassluis Formation. Borehole De Meern shows the interdigitation of the Waalre Formation and the Peize Formation, while Borehole Hipolytushoef is mainly dominated by the Peize Formation. This is because of the different fluvial impact from the south (Rhine-Meuse system) and the east (Eridanos system). With regards to the lithology of Petten Borehole 1, we can generally expect a higher similarity to Borehole Hipolytushoef, which shows stronger impact from Eridanos system than Rhine-Meuse system. Several features can also be expected in the lower half of the Petten Borehole 1. The overall sediment could show the trend of coarsening upwards, while the sand to clay cycles do exist throughout the core. As the Maassluis Formation and the Peize Formation are in part contemporary, we might see water depth changes at the transition between these two formations. Even if there is no apparent interdigitation of the Peize Formation and the Waalre Formation, we could still witness more Rhine-Meuse signals upwards the Peize Formation by heavy mineral investigation. Sedimentary hiatus in the Peize Formation should also be drawn attention to, since the deltaic area of Eridanos river system experienced repeatedly erosion events.

3. Materials and Methods

3.0 Petten Borehole 1 and the Prior Study

The Petten Borehole 1 was extracted by GeoSonic Drilling, Ltd. In 2018, and was drilled on the premises of Pallas in Petten (N=107205.580, E=533419.566 in min RD, or 52.786° N, 4.679° E in GPS coordinates). The core reaches a terminal depth of 381.15 m, with the top an elevation of 3.26 m above NAP (Dutch ordnance datum, ≈ MSL). Sonic drilling was performed down to 101.5 m depth, and wireline rotary coring was performed below that. The upper section of the core (0 – 101.5 m) is almost completely recovered, while the lower section has substantially lower recovery. TNO Geological Survey of the Netherlands acquired the cored materials after the drilling, together with lithological descriptions and gamma ray log (GR) records. After acquisition, TNO, in cooperation with Utrecht University, set up a dating project to develop the age model for the core, making use of paleomagnetism and palynology.

Paleomagnetism / Magnetostratigraphy

97 samples were taken for paleomagnetic analyses at the Fort Hoofddijk laboratory (UU), using alternating field demagnetization, while the results were thought affected by secondary greigite growth. Therefore, another 65 samples were taken to redo the paleomagnetic analyses using thermal demagnetization. Fine-grained lithologies (silt, clay) were preferentially chosen for the analyses, and the samples were taken from the interval 221.33 – 383.01 m.

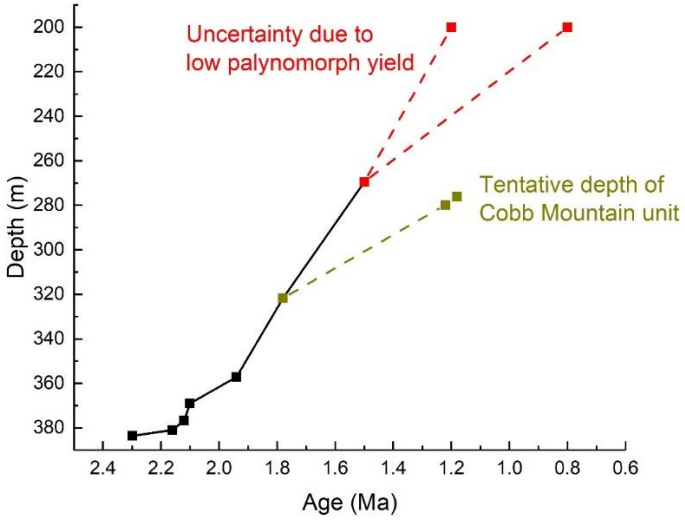

Figure 4 *Black solid line shows the preliminary age model of the Petten Borehole 1 based on paleomagnetic and palynological tie-points from prior study by TNO. Red dashed lines indicate a range of age of 200 m depth due to low palynomorph yield. Green dashed line presents part of the age model based on tentative depth of Cobb Mountain paleomagnetic unit.*

Palynology / Biostratigraphy

46 samples were taken for palynological analyses. In order to yield sufficient palynological materials, the main focus was on the interval below 200 m depth (32 of 46 samples) which is the section with finer lithology. Houben (2019) indicated in the report that the base of Petten Borehole 1 is to be placed in the Early Pleistocene, middle Gelasian (2.3 – 2.1 Ma). Higher up in the core, the following chronostratigraphic tie-points were implied from the paleomagnetic and palynological analyses: 380.91 m

is corresponding to 2.16 Ma, 376.72 m to 2.12 Ma, 357.12 m to 1.94 Ma, and 321.70 m to 1.78 Ma (**Figure 4**).

A Middle Pleistocene age (0.8 – 1.2 Ma) is interpreted at about 200 m, but from this level upwards there is generally poor preservation of palynological materials in coarser lithologies.

Considering the recovery condition and the grain size distribution, the MSc project (this thesis research and the parallel palynological thesis research) chose the interval below 195.45 m of the Petten Borehole 1 as the study section. This was to raise the possibility that the samples could yield enough palynomorphs to conduct palynological analyses. Also, this interval is dominated by medium sand, which helped confine the heavy mineral analysis within one lithology and make the results comparable.

3.1 Lithological-Sedimentological Logging, including Water Depth Estimation

The lithological descriptions by the original contractors of Petten Borehole 1, were based on the materials sampled every two meters on average. In this thesis research, the section from 195.45 – 384.05 m was relogged at higher resolution, for lithological and sedimentological criteria. This has resulted in a lithological-sedimentological dataset with a resolution of ca. 4 observations / meter on average.

For the lithological logging, we have gone through the core twice to record the information. The first run aimed to divide the core into smaller units, based on the lithology (sand, silt and clay) and color. The units were in meter level, and each unit was assigned with a code, which consists of letters and numbers. The letters represent five categories including S (sand), Si (silt), C (clay), M (mixed), P (peat), and the numbers of each category are in an order from the top (shallow) to the bottom (deep). Note that the term ‘mixed’ here means both homogeneous and heterogenous, and the mixed units were elaborated in the second run. Samples were taken every meter or whenever the lithology changed abruptly. Dominant grain size ranges and intuitive colors were recorded, and other obvious sedimentary features (preserved shells, peat, bioturbation, etc.) were also noted if present. Grain size ranges were determined by a grain size comparator, where the samples were described as clay, silt, fine sand (50 – 75 µm, 75 – 105 µm, 105- 150 µm), medium sand (150 – 210 µm, 210 – 300 µm, 300 – 420 µm), and coarse sand (420 – 600 µm, > 600 µm).

The second run further increased the resolution of the lithological logging into

decimeter level and added description details, including sedimentological interpretation (see below). During this run, we also took 3 to 4 samples every meter or whenever the lithology changed abruptly. 40 times magnifying binoculars were used to note down the roundedness of the deposition, classified by very angular, angular, sub-angular, sub-rounded, rounded, and very rounded. Also, the color of the sample (in the semi-dried state that the core was stored in) was specified following the Munsell Color System, using the 10YR chart.

Sedimentological descriptions were conducted alongside the lithological logging, and were checked on the core afterwards when necessary. The descriptions were based on the alternation of lithologies and grain size change. We mainly noted down the tidal condition (subtidal/intertidal zone) when the deposition was tide-dominated, and relative water depth change. The water depth estimation was first based on sedimentological observations, including tidal stratification and pedology. It was then cross-checked by other evidences and results. The estimation was iterated by looking up and down along the core (i.e. putting the individual samples in a larger context), cross-checking with grain size and geochemical results (see below), and cross-checking with observations on macrofossils (shells, bioturbation) and microfossils (parallel palynological results). Also, age model was taken into consideration, where the sedimentation rates and sedimentary hiatus might give the insight into relative water depth change (e.g. shallowing process). Estimated values of water depth were given to each individual observations (approximately every 5 meters). Note that the values in this study aimed to reveal relative water depth change and the trending throughout the core, so the exact values might not be precise. Also, due to the relatively low resolution of our observations, not all relevant paleoclimate features (e.g. 41-kyr glacial-interglacial cycles) can be presented.

3.2 Grain Size Analysis

The grain size analysis aimed to identify the grain size distribution in the selected samples, and we needed to split the samples based on several grain size ranges. 21 samples were taken preferentially from the interval 195.45 – 384.05 m (**Table 1**). This set of samples was used to perform grain size analysis, heavy mineral analysis, and also part of element concentrations measurement, so we preferentially sampled the medium sand lithology to avoid potential deviation in the heavy mineral analysis that might be resulted from finer grains. Each sample contains approximately 100 g

materials.

Table 1. Selected sample positions for grain size analysis, heavy mineral analysis, and part of element concentrations measurement.

Depth down core (m)		
201.88	262.22	339.7
220.75	269.02	345.22
222.7	283.85	353.34
230.7	288.4	359.75
240.88	298.8	366.15
250.22	314.77	369.12
255.83	328.62	378.23

The samples were placed in 250-ml or 300-ml beakers for pre-treatments. First, we removed $CaCO_3$ and Fe coatings with hydrochloric acid (HCl). 5% HCl was added roughly to 200 ml level of each beaker. The samples were stirred thoroughly and placed on hot plate (105 degrees Celsius set) overnight to accelerate the reaction. We changed the liquid in the beaker with fresh HCl and repeated the step twice. For the samples with lots of shells, we repeated even more times to remove all $CaCO_3$. Samples were then washed with demineralized water and placed overnight until all the particles were settled down. All samples were washed three times to make sure little HCl was remained in the beakers.

Second, we removed the organic materials with hydrogen peroxide (H_2O_2). 30% H_2O_2 was added roughly to 150 ml level of each beaker. The samples were stirred thoroughly and placed on hot plate (105 degrees Celsius set) overnight to accelerate the reaction. We changed the liquid in the beaker with fresh H_2O_2 and repeated the step twice. For the samples with lots of organic materials, we repeated even more times to remove all of them. Samples were then washed with demineralized water and placed overnight until all the particles were settled down. All samples were washed three times to make sure little H_2O_2 was remained in the beakers.

Samples were firstly split at 53 μm, and further separations were then performed in < 53 μm fraction (silt and clay) and > 53 μm (sand) fraction. To split the samples at 53 μm, we prepared a funnel rack with a 53-μm sieve right on the funnel and a 1-L column below. Demineralized water was added roughly to 150 ml level of a sample

beaker. We stirred the sample thoroughly and let the beaker stand still for 10 seconds. The liquid with suspended materials in the beaker was then poured on the sieve. This step was repeated several times until the liquid in the beaker was clear after 10-second standing still. The residual particles on the sieve was washed back to the beaker with demineralized water. All 21 samples were split at 53 μm in this way, and thus the silt and clay fractions were in columns whereas the sand fractions were still in beakers.

We separated the fraction finer than 53 μm into 5 ranges (< 2 μm, 2 – 8 μm, 8 – 16 μm, 16 – 32 μm, and 32 – 53 μm). Separation in this fraction utilized the Stokes' law. Stokes' law is an expression for the frictional force exerted on spherical objects with small Reynolds numbers moving through a viscous fluid, which is given by:

$$F_d = 6\pi\,\eta\,r\,v$$

F_d is the frictional force; η is the dynamic viscosity of the fluid; r is the radius of the spherical object; v is the flow velocity relative to the object. One of the applications of the Stokes' law is to determine the terminal velocity of a small particle falling in a fluid, which is widely used in sedimentation modeling. The excess force F_g on the falling particle in the fluid is given by:

$$F_g = (\rho_p - \rho_f)g\,\frac{4}{3}\pi\,r^3$$

ρ_p is the density of the particle; ρ_f is the density of the fluid; g is the acceleration of gravity. The particle requires the force balance $F_d = F_g$ to reach the terminal velocity, and thus this velocity v can be given by:

$$v = \frac{2r^2}{9\eta}\,g(\rho_p - \rho_f)$$

The travel distance h of the particle after t seconds can be further given by:

$$h = v\,t = \frac{2r^2}{9\eta}\,g(\rho_p - \rho_f)t$$

In this analysis, we exploited 2.65 g/cm^3 for the density of the particle (as the major constituent of the sediments is quartz with the density of 2.65 g/cm^3), 1 g/cm^3 for the density of demineralized water, and 981 cm/s^2 for the acceleration of gravity. Temperature has an impact on the fluid viscosity, so the travel distance h is a function of the temperature (**Table 2**). The travel distance showed in **Table 2** instructed the separation in the fraction finer than 53 μm. As the temperature in the laboratory was holding between 21.0 ℃ and 21.5 ℃, numbers followed in these two rows were used.

Table 2. Travel distance (cm) of the particle falling in demineralized water as a function of the temperature following Stokes' Law.

t (℃)	η (poise)	t = 10 s, $2r$ = 53 μm	t = 4 min, $2r$ = 32 μm	t = 16 min, $2r$ = 16 μm	t = 30 min, $2r$ = 8 μm	t = 16 h, $2r$ = 2 μm
20.0	0.01009	21.9	21.9	21.9	10.3	20.5
20.5	0.00997	22.2	22.2	22.2	10.4	20.8
21.0	0.00984	22.5	22.5	22.5	10.5	21.1
21.5	0.00972	22.7	22.7	22.7	10.7	21.3
22.0	0.00961	23.0	23.0	23.0	10.8	21.6

Demineralized water was added exactly to 1 L level of each column with silt and clay fractions. 0.8 g Natrium Pyrophosphate ($Na_4P_2O_7$) was added to each column to disaggregate the sediment. We shook the columns thoroughly and waited 30 minutes for the disaggregation process. Then we shook the columns again and waited for a certain time as given in **Table 2**. A pipette was used to extract 25 mL of the turbid liquid at the depth given in **Table 2**, and the liquid was then moved to weighed stainless cups and placed in the oven overnight. The dried cups were also weighed afterwards. In this way, we could collect the 1/40 (25 mL/1 L) weight of silt and clay fractions in 5 ranges (< 53 μm, < 32 μm, < 16 μm, < 8 μm, and < 2 μm). We firstly performed the extraction of the materials with < 53 μm range and then to the finer fractions, in order to remain the concentrations of finer particles in the column for the latter extractions.

Separation in the fraction coarser than 53 μm simply used the sieves. The materials remained in the beakers were moved to weighed stainless cups, and placed in the oven overnight. We selected and weighed 11 different sieves (1000 μm, 850 μm, 600 μm, 500 μm, 425 μm, 300 μm, 212 μm, 150 μm, 106 μm, 75 μm, and 53 μm) and a base holder. Each dried sample of sand fraction was sieved by these sieves using a sieving vibrator. The sieves were weighed again to collect the weight of different fractions. Note that the base holder might obtain some materials which went through the 53-μm sieve, and this weight was added to the 32 – 53 μm fraction of this according sample.

16 grain size ranges (> 1000 μm, 1000 – 850 μm, 850 – 600 μm, 600 – 500 μm, 500 – 425 μm, 425 – 300 μm, 300 – 212 μm, 212 – 150 μm, 150 – 106 μm, 106 – 75 μm, 75 – 53 μm, 53 – 32 μm, 32 – 16 μm, 16 – 8 μm, 8 – 2 μm, and < 2 μm) of each sample were presented in weight (g). They were also calculated in weight percentage

for a more straightforward comparison.

3.3 Heavy Mineral Analysis

A heavy mineral in the sediment is a mineral with a density greater than 2.89 g/cm^3. Heavy mineral analysis aimed to determine the kinds and content of different heavy minerals in a sediment sample. Different heavy mineral suites can indicate different provenance and history of the deposition. We chose a range of grain size (53 – 500 μm) to perform the analysis in order to make the results from different samples comparable. The samples should be pre-treated the same way as grain size analysis to remove $CaCO_3$ and organic materials, so the 53 – 500 μm fractions of each sample were collected from the sieves (425 μm, 300 μm, 212 μm, 150 μm, 106 μm, 75 μm, and 53 μm) after the sieving process for grain size analysis. They were placed in stainless cups.

In order to separate heavy minerals from the other sediments, we made use of the heavy liquid made from sodium polytungstate ($Na_6[H_2W_{12}O_{40}]$) to float the light materials and sink the heavy minerals. The heavy liquid was adjusted exactly to a density of 2.89 g/cm^3. A funnel rack was prepared, together with a large funnel with a screw-like switch, several small funnels and filter papers. The separations of heavy minerals of each sample were performed one by one. 150 mL heavy liquid was added in the large funnel with the switch off, and 10 g of the pre-mixed sample (53 – 500 μm) was added to the heavy liquid. The heavy liquid was then stirred thoroughly and waited for about 20 minutes until the heavy minerals were all settled down above the funnel switch. We turned on the switch and released about 1 cm of the liquid into an evaporating cup. The heavy minerals in the evaporating cup were washed several times first with demineralized water to remove the salt, and second with ethanol to quickly remove the water. The cup was then placed on the hot plate and dried. The dried heavy minerals were carefully collected into a plastic vial. The isolated portion of heavy minerals was weighed and expressed as weight % of the 53 – 500 μm grainsize fraction of the sample. Note that the heavy liquid was recycled by filtering and evaporating. The heavy mineral counting was carried out with the transmitted-light polarizing microscope. Resin was used as the medium to make have mineral slides.

3.4 Element Concentrations (XRF)

Element concentrations in the sediment provide more information about the

sedimentary history, and could help reconstruct the paleoenvironment. The concentrations can be acquired by X-ray fluorescence (XRF) measurement. XRF is the emission of characteristic fluorescent X-rays from a material that has been excited by being bombarded with high-energy X-rays. We used an Olympus XRF analyzer (Delta Premium – 50 kV) to measure the element concentrations in our samples. The default program for soil was used in the measurement, which detected the concentrations of P, S, Cl, K, Ca, Ti, Cr, Mn, Fe, Co, Ni, Cu, Zn, As, Se, Rb, Sr, Zr, Mo, Ag, Cd, Sn, Sb, Ba, Hg, and Pb.

73 samples in total were taken to perform the element concentrations measurement, of which 21 samples were pre-treated and 52 samples were not pre-treated. The 21 pre-treated samples were the same materials as the fractions collected for heavy mineral analysis, and thus only contained the grains with the size range 53 – 500 μm. 21 of the 52 untreated samples were taken from exactly the same depth as the 21 pre-treated samples (**Table 1**), and the other 31 samples were taken in order to reach a sequence of element concentrations with higher resolution (**Table 3**). These 31 samples were taken from all lithologies (sand, silt and clay).

Table 3. Selected sample positions for extra element concentrations measurement.

Depth down core (m)			
208.3	264.55	305.1	342.75
213.1	272.25	308.65	349.5
225.65	276.2	312.6	357.85
227.25	279	320.75	363.05
243.85	285	325.3	374.2
247	287.45	327.25	376.87
253.8	293	333.4	379.95
258.55	302.15	336.4	

The 21 pre-treated samples were already dry and loose, which were ready for the XRF measurements. The measurements were performed one by one. About 10 g of each sample was added and filled a special plastic capsule and covered by a plastic foil. The capsule was then detected by the XRF analyzer. All the 52 untreated samples were first placed in the oven overnight to get dried. Aggregate samples were crushed into finer material. Shells were also presented in some of the samples, and were

crushed into mm-scale pieces. The measurements for these 52 untreated samples were the same as treated ones.

3.5 Other Information

Another 533 samples were taken from the study interval of the Petten Borehole 1 (195.45 – 384.05 m), which were used for the palynological study in the parallel MSc thesis by Krom. These samples were taken from all lithologies (sand, silt and clay), but preferentially from the finer fractions to yield sufficient palynomorphs for analyses. Krom generated palynological sequences based on pollens, spores, dinocysts and foraminifera from these samples, and part of the results are also used in this thesis (Chapter 5 and 6) for a more integrated interpretation and discussion. The reader is referred to the parallel MSc thesis by Krom for methodological details.

4. Results

4.1 Lithology and Sedimentology

After the first run of lithological logging, the studied section of core (195.45 – 384.05 m) was divided into 159 meter-resolution units, including 77 sand units, 31 silt units, 42 clay units, 8 mixed units and 1 peat unit. At that resolution of logging, each unit might contain other lithologies than the assigned dominant attribution. Grain size of sand fractions generally ranges from 50 to 600 μm, showing a coarsening upwards. The top 50 m of the studied section basically presents the sand with medium grain size (150 – 420 μm), while the rest mostly showing fine sand fractions (50 – 150 μm). Accordingly, only very few silt and clay units exist in the top 50 m (above 250 m depth), and the finer lithologies are more dominant in the rest of the studied section.

Preserved shells are spotted in the lower half of the study section, as small individual specimen. Shell fragments occur in sand or silt lithologies. Besides the single meter-scale peaty unit, thinner intervals of peats and reworked clasts of peat appear at various levels throughout the studied section. The interval 256 – 261 m is the most peaty one (more than 80%). Bioturbations can also be found in the core, especially in the bottom 10 m of the study section. Pictures of special sediment structures and evidences, including shell fragments and bioturbations, can be found in **Appendix 1**.

The second run of lithological logging brought its resolution to decimeter level. The

lithological characterization was also upgraded, as part of selecting intervals for taking samples for the lab analysis. Grain roundness was logged for the sand fraction, which ranges from very angular to rounded. The roundness does not show an obvious pattern throughout the study section. Color of the sediment was also recorded using the 10YR chart of Munsell Color System. In the semi-dried state, color of the sand units in the lower half of the study section generally falls in 5-7/1-2, which is described as grey to light brownish grey. In the upper half, the sand mostly shows color of 5-7/2-3, which is described as brown to pale brown. That is to say the sand units generally present a more-yellowish-upwards pattern. For the silt and clay units, the colors are darker, in a range of 3-4/1-2, described as very dark grey or dark grey. Some silt and clay units in the upper half, however, can reach a brighter value of 5/1 or 6/1, described as grey. In addition, sporadic black minerals are spotted in sand units throughout the study section.

Sedimentological logging was conducted mainly focusing on energy change of sedimentary environment and tide-relative depositions. Very thin alternations of coarser and finer depositions exist in 270 – 335 m, which are interpreted as sub-tidal or intertidal formations. Also, we noted down a generally increasing energy level of the sedimentary environment throughout the study section by the coarsening-upwards sand fractions. These sedimentological information helps the water depth interpretation in the next chapter. Concerning the sedimentology, we also sorted out all the units in the lithological logging and made a less-detailed series of lithological units (**Figure 5a**), which remains the basic lithological information and shows the major change of the sedimentary environment.

4.2 Grain Size Analysis

Laboratory grain size analysis was conducted over the 21 selected and treated samples, targeting 16 grain size ranges (sieving meshes). The weights of each range were recorded and the percentages calculated from this. In the raw measurements, there are 5 non-positive values of weight percentage in the silt and clay fractions of sample 6, 12, 13 and 14, which might be due to experimental error. These values could be negligible as the samples were intentionally picked from sand lithology, and sand is the dominant constituent. The curve of mean grain size against the core depth is shown in **Figure 5b**. Three ternary diagrams of grain size distribution are shown in **Figure 6**. Clearly we can see every sample contains more than 90% sand. Medium sand is the main constituent within the sand fraction, whereas fine sand dominates in some

samples. Only very few samples contain trace of coarse-grained sand, as shown in **Figure 6c** that the dots mostly fall on or near the right axis. There is not significant difference of grain size composition among different core depths.

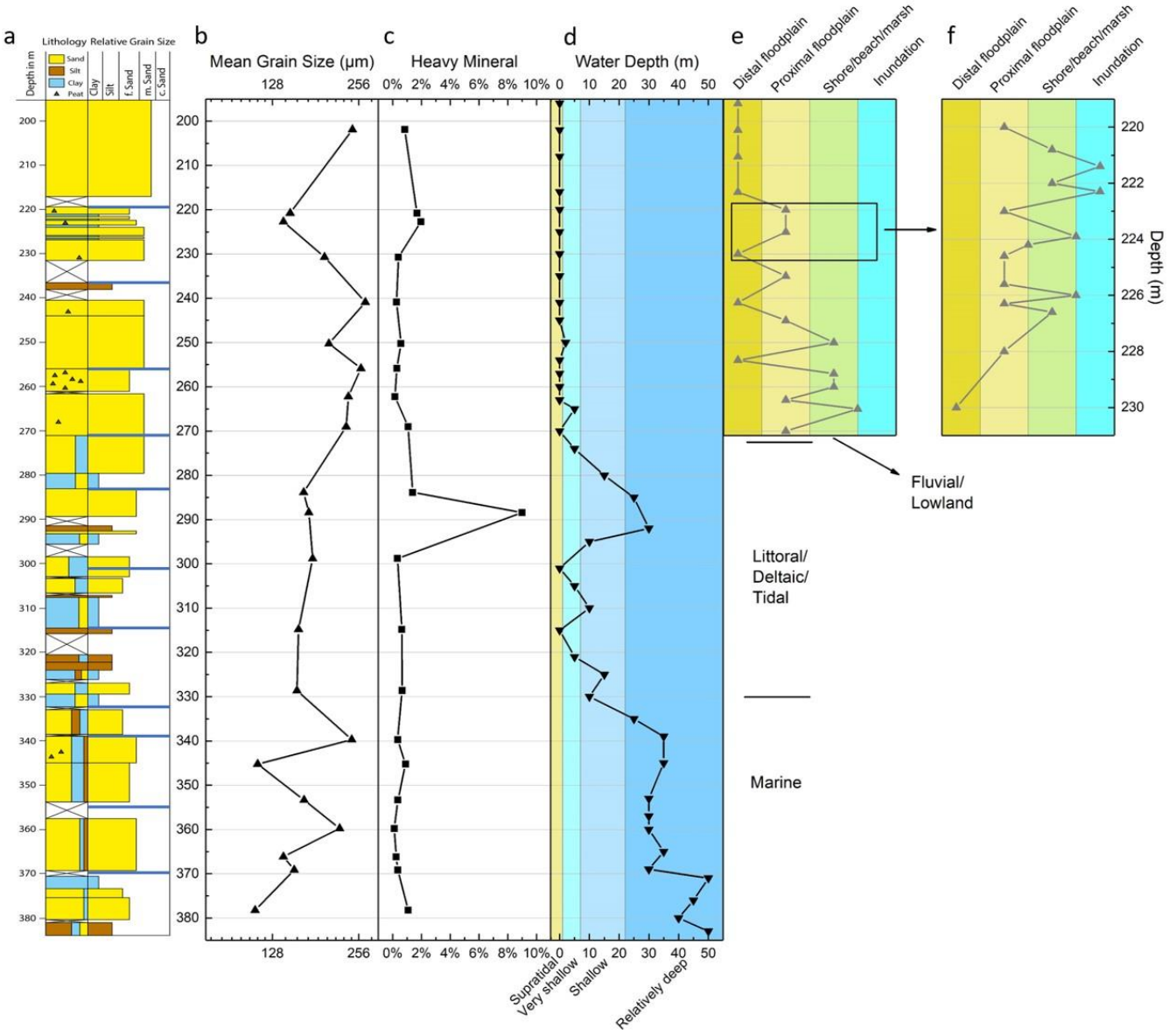

Figure 5 a *Lithology of the Petten Borehole 1 (195.45 – 385.05 m) made in this study. Compositions of each unit and peat evidences (as beds or clasts) are also indicated. Secondary divisions used in Chapter 5.2 are presented in blue lines.* ***b*** *Mean grain size against core depth (% weight based). Note that the grain size range of > 1000 μm is not included in the calculations.* ***c*** *Heavy mineral weight percentage.* ***d*** *Estimated water depth based on sedimentological logging.* ***e*** *Fluvial environment change in the upper part of the core.* ***f*** *Fluvial environment change in the interval 220 – 230 m.*

Grain size frequency curves of the 21 samples are shown in **Figure 7**. Medians of each grain size range are plotted on a logarithmic x-axis. All the samples have peak values at ranges of 106 – 150 µm, 150 – 212 µm or 212 – 300 µm. Almost all the samples are single peaked. Sample 5 is the only one showing two peak values, at 106 – 150 µm and 212 – 300 µm respectively. For the single-peaked curves there are two modalities: positive and negative skewness. If the finer fraction dominates the grain size range, the grain size distribution is described as negatively skewed. Accordingly, positive skewness describes that the coarser fraction than the dominant grain size range is more than the finer fraction. In our grain size frequency curves, sample 1, 2, 4, 6, 7, 8, 12, 13, 14 and 19 show negatively skewed curves, while sample 15, 16, 17, 18 and 20 show positively. Sample 3, 9, 10, 11 and 21 are quasi-normally distributed, but showing a weak negative skewness. In general, samples from deeper section of the core tend to show negative skewness (**Figure 8**).

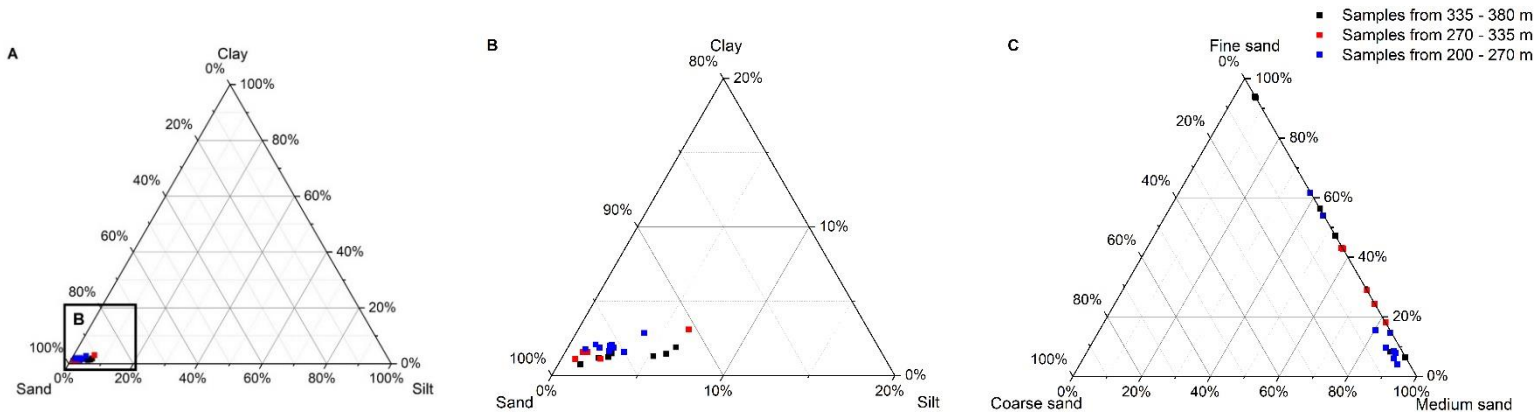

Figure 6 a,b *Ternary diagrams showing the grain size distribution of 21 samples.* ***c*** *Ternary diagram showing the grain size distribution of the sand fraction. (Clay: < 2 µm; silt: 2 – 53 µm; fine sand: 53 – 150 µm; medium sand: 150 – 425 µm; coarse sand: > 425 µm sand)*

4.3 Heavy Mineral Analysis

The heavy mineral concentrations (weight percentages of fraction 53 – 500 µm) of 21 samples are shown in **Figure 5c**. The weight percentages range from 0.1% to 2%, with sample 11 (288.4 m) showing a 9%. The average weight percentage of these 21 samples is 1.09% including sample 11, and 0.69% excluding sample 11. There is no significant trending of the heavy mineral weight percentages throughout the core. Also, no obvious pattern can be described due to the relatively low resolution.

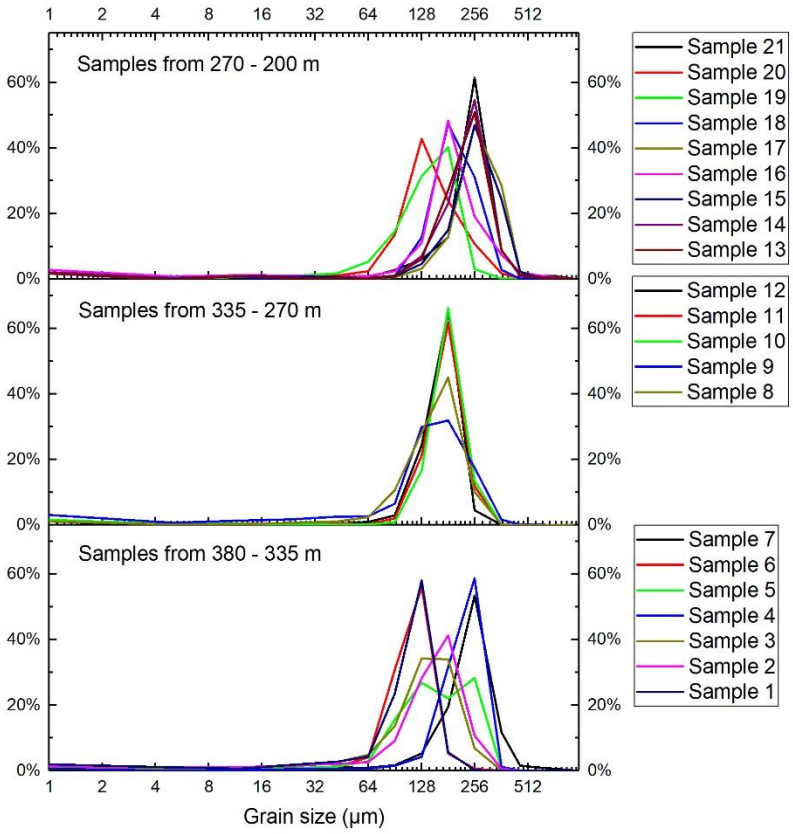

Figure 7 *Grain size frequency curves of 21 samples. Note that the grain size range of > 1000 μm is excluded.*

4.4 Element Concentrations

Element concentrations of 52 untreated samples are presented in this chapter. Among all the detectable elements, S, Cl, K, Ca, Ti, Cr, Fe, Zn, Rb, Sr, Zr, Ba and Pb are continuously detected. Mn is also continuously detected, except in one sample. Concentrations of selected elements together with some ratios of two elements are shown in **Figure 9**.

Of the selected elements in the figure, Zr, Rb and Sr remain below 2000 ppm, and are regarded as trace elements. Ti and Zr, sharing similar patterns, show good correlations with heavy mineral content. The r^2 of the correlation between Ti/Zr and heavy mineral content of the 21 samples are 0.838 and 0.867 respectively. Therefore, we can roughly use Ti or Zr concentrations as indicators of heavy mineral contents at the depth where heavy mineral analysis was not conducted. Rb and K have anticorrelations with grain size, which means the larger grain size of the sample, the

lower values of Rb and K. The r^2 of the correlation between Rb/K and weighed mean grain size of the 21 samples are 0.514 and 0.519 respectively. Thus Rb and K can be described as grain size sensitive and should be noticed when doing the interpretation. From the curves we can see that Fe has a similar pattern to that of Rb or K, but the r^2 of the correlation between Fe and weighed mean grain size is only 0.123, indicating Fe is also subject to other conditions than grain size variation. S concentration co-varies with Fe in the interval 280 – 380 m (r^2 = 0.554), while it co-varies with Ba in the interval 200 – 280 m (r^2 = 0.854). This can be clearly observed from the figure. Ba and Ca each has one prominent peak value respectively at 264.55 m and 314.77 m, where exactly Sr shows its two prominent peaks in the curve. In addition, Sr concentration has a better correlation with Ca in the interval 280 – 380 m (r^2 = 0.837), while having a better correlation with Ba in the interval 200 – 280 m (r^2 = 0.783). Ratios of Ca to Sr and Zr to Rb are presented in the figure. All of the element concentrations and ratios are further interpreted in the next chapter.

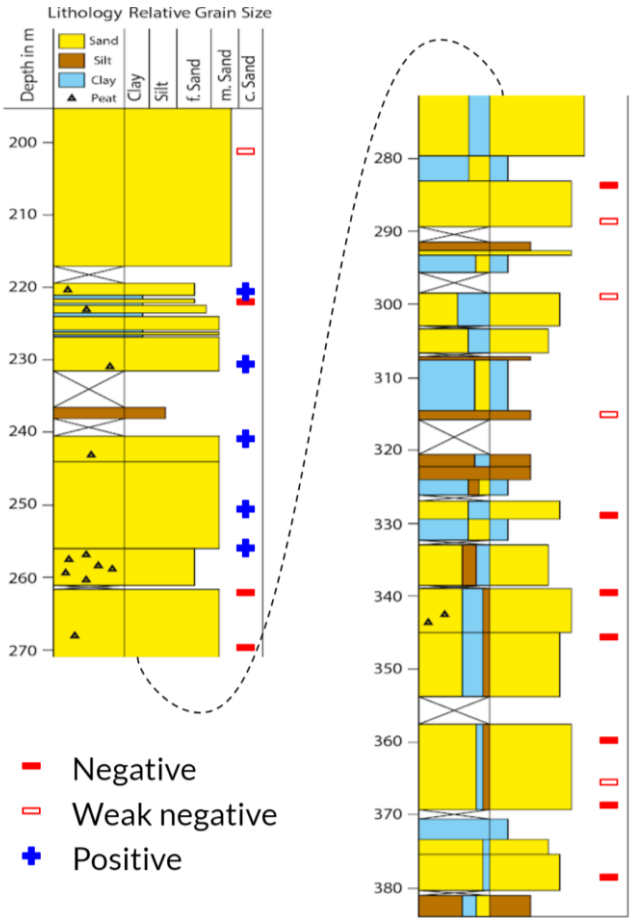

Figure 8 *Skewness of grain size distribution of the 20 samples with the depths (excluding Sample 5 at 353.34 m)*

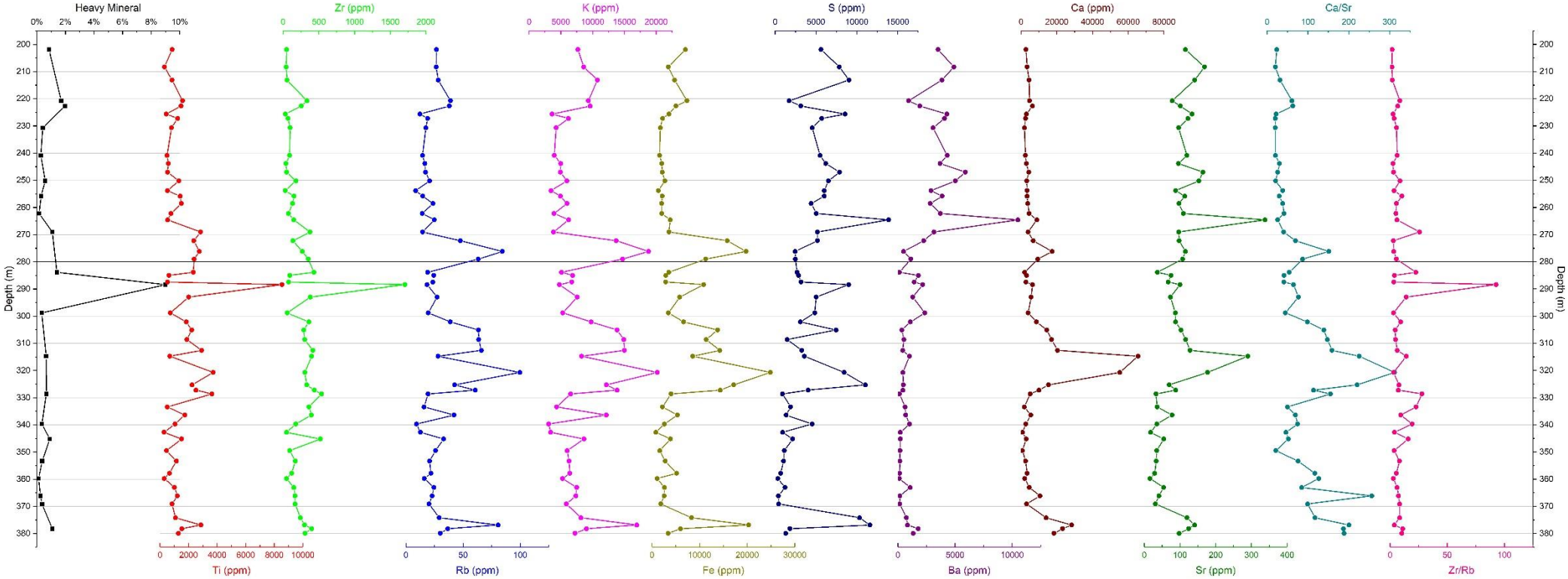

Figure 9 *Heavy mineral concentration (weight % of 53 – 500 µm fraction; 21 samples) and selected element concentrations and ratios from XRF measurements (52 samples).*

5. Interpretation

5.1 Sedimentary Environment Indicators

5.1.1 Geochemistry

Geochemical proxies (i.e. elements and their ratios) in the core sediment have been long investigated for paleoclimate study (Rothwell, 2015). The trending of each element and their correlations can help us determine or narrow down the sedimentary environment in different depth intervals. As presented in the Results chapter, here we interpret the selected elements, ratios and their correlations shown in **Figure 9**.

Titanium (Ti) and Zirconium (Zr)

Ti tends to be enriched in coarse-grained fraction, and it is generally representative for terrigenous sediments (Rothwell, 2015). Therefore, Ti is used to record terrigenous sediment delivery, and thus an indicator of hinterland climate (e.g. Haug et al., 2001; Peterson et al., 2000). Ti basically occurs in heavy minerals like rutile (TiO_2), anatase (TiO_2) and ilmenite ($FeTiO_3$). Zr also varies with coarse-grained fraction, and it mainly occurs in zircon ($ZrSiO_4$). Both Ti and Zr might be high in ash layers (Rothwell, 2015).

The good correlations between heavy mineral content and Ti/Zr (**Figure 9**) also support the occurrence of Ti and Zr in heavy minerals. Besides, the trendings of Ti and Zr can be roughly used to estimate the heavy mineral content throughout the core. Ti concentration is approximately four times Zr concentration, which can indicate the relative abundance of rutile/anatase/ilmenite (if there) and zircon. The sample taken from 288.4 m (Sample 11) shows a weirdly high value for heavy mineral content, Ti and Zr. The position of 288.4 m in the core clearly shows two black sandy layers, and the grain size of the sediment does not change much within the +/- 10 cm interval. This could be interpreted as volcanic events or sediment-reworking-caused heavy mineral concentration. Further interpretation requires analysis of the heavy mineral composition. We can also observe that both Ti and Zr vary more heavily in the lower half of the core. This is because the lithology is more diverse in the lower half, where we can sample from different lithologies, while the upper half mainly contains massive sand. Ti and Zr tend to be enriched in coarser fractions, which results in the zigzagging curves of Ti and Zr in the lower half, especially Ti.

Rubidium (Rb) and Zr/Rb

Rb is widely dispersed in the nature, but seldom forms distinct mineral species (Rothwell, 2015). Therefore, the strong positive correlation between decreasing grain size and increasing trace element concentrations (Horowitz, 1991) makes Rb a good grain size indicator. Concerning Zr enriched in coarse-grained fraction, the ratio Zr/Rb can also be a grain size proxy. However, the sample from 288.4 m, showing weirdly high Zr concentration, has disturbed grain size indication of Zr, and thus the curve of Zr/Rb also shows a high value at 288.4 m but a much lower amplitude elsewhere. In this case, Rb itself is a much better grain size proxy. Rb mainly has three peaks throughout the core at 276.87 m, 320.75 m and 276.2 m, and all these three samples are taken from silt or finer lithologies. Similar to the curves of Ti and Zr, more zigzags are shown in Rb from 270 m below, which is also resulted from the more diverse lithology in the lower interval.

Potassium (K) and Iron (Fe)

K is generally associated with terrestrial siliciclastics, especially with illite clays (Rothwell, 2015). This makes K enriched in fine sediment fractions, and the similarity between Rb and K observed in **Figure 9** can support that. Fe also shows a similar pattern with Rb and K, but Fe has a more complicated characteristic, and thus cannot be simply interpreted as grain size sensitive. Fe is a terrigenous indicator like K, but it is also redox sensitive and can relate to dilution of $CaCO_3$ (Rothwell, 2015). Fe is prone to diagenetic remobilization. For example, greigite (Fe_3S_4) can be formed diagenetically in some sedimentary environments, including some coastal sedimentary settings. Houben (2019) confirmed that in-situ magnetic minerals have hampered further interpretation for magnetostratigraphy using alternating field demagnetization in the Petten Borehole 1, and greigite is believed to be responsible. Considering that the sedimentary environment might contain shallow marine to lowland, more geochemical information should be put together to further interpret the change of Fe, including considerations shared with Sulphur, discussed in the next section.

Iron (Fe), Sulphur (S) and Barium (Ba)

S is closely associated with organic materials (i.e. marine plants), and can be buried in their dead remains as mineralized S (Rothwell, 2015). S can also be formed in a reduced iron sulphide phase, and thus can be an proxy of reducing condition. In this case, high S an Fe indicate a suboxic or anoxic environment (e.g. Sluijs et al.,

2009). Ba has been widely used as a marine productivity proxy (e.g. Ziegler et al., 2009). However, Ba can be dissolved in suboxic or anoxic environment by sulphate depletion (e.g. van Os et al., 1991). So multi-proxy approach is required to reconstruct the productivity.

In **Figure 8**, S co-varies with Fe in the interval 280 – 380 m, while co-varies with Ba in the interval 200 – 280 m. The good correlation between S and Fe in the lower part reveals that S and Fe are mostly in the form of reduced iron sulphide (FeS), indicating this interval experienced suboxic or anoxic environment. The sub-intervals showing both high S and Fe (~ 290 m, ~ 305 m, 320 – 330 m, 370 – 380 m) should be associated with even stronger reducing condition. The slight offset of the co-variation of S and Fe is due to either partial S in the form of sulphate or terrigenous detritus input of Fe. On the other hand, Ba remains at a low level and small amplitude in the lower part compared to the upper part. This is because of the Ba dissolution by sulphate depletion in the reducing environment. The good correlation between S and Ba in the upper part indicates that S has changed its main form of existence. As S lost the connection with Fe, representing the weakening of reducing condition, and built a new firm correlation with Ba, it is very likely that S is then in the form of biogenic barium sulphate ($BaSO_4$). In this case, S and Ba can be regarded as productivity proxies in the upper part. The variation of Fe in the upperpart might then be an indicator to other conditions, e.g. terrigenous input. But it does not provide much information considering the small amplitude of variation.

Barium (Ba), Calcium (Ca), Strontium (Sr) and Ca/Sr

As said that Ba alone is not sufficient to reconstruct the productivity, here we present two more elements as productivity proxies. Ca is mainly biogenic or detrital (Rothwell, 2015). Biogenic Ca basically exists in the form of $CaCO_3$, representing the oceanic productivity. Detrital Ca (mainly transported and enriched in the silt fraction) is remarkable in near-shore and deltaic area, and hence is important in this study. Ca also has limitations being a productivity proxy, because it can be subject to carbonate dissolution (e.g. in acidic environment induced by rain or humus, which is believed to occur above 280 m of this core) and/or dilution by terrigenous material (Rothwell, 2015). Compared to Ba and Ca, Sr is a more steady productivity proxy. Sr is fixed by calcifying organisms at the same time as Ca, and thus it is a marker of biogenic origin. Given the same formation process of Sr and biogenic Ca, co-variation of Sr and Ca can indicate

that Ca is mainly sourced from biogenic $CaCO_3$. High Ca/Sr can then reveal a high detrital Ca and low biogenic Ca situation (e.g. Hodell et al., 2008). Also, Sr is prone to be associated with aragonite, and thus can be used to distinguish foraminiferal calcite and coralline and/or pteropod aragonite (e.g. Richter et al., 2006).

It is apparently that Sr co-varies better with Ca in the interval 280 – 380 m, and better with Ba in the interval 200 – 280 m. Ba in the lower part and Ca in the upper part share a similar pattern, which both vary at a lower level and smaller amplitude. Suboxic and anoxic environment existing in the lower part, as mentioned previously, leads to the depletion of Ba, which makes Ca and Sr good indicators of productivity there. Either dissolution of carbonate or dilution by terrigenous material is responsible for the low Ca value in the upper part. But since Ba and Sr do not show a diluted signal and still vary at an informative level, it is more possible that $CaCO_3$ is subject to dissolution in some intervals of the upper part (as the low values of Ca shown in **Figure 9**). This likely indicates a delta plain sedimentary environment to have established at this point in the Early Pleistocene, in which deposits were subaerially exposed and acidity from precipitation dissolved the $CaCO_3$ as soils developed on the delta plain. Ca/Sr can help determine the content of detrital or biogenic carbonate. But it is very interesting that the ratio varies more heavily in the lower part, where Ca and Sr actually show good correlation. Comparing the ratio with other terrigenous-indicating elements (e.g. K, Fe), they do share similar patterns to some extent. In addition, relatively high values of the ratio (e.g. 276.2 m, 320.75 m and 376.87 m) are mostly from the finer samples (with more silt fraction), which also conforms to the enrichment of detrital Ca in the silt fraction. It means Ca/Sr can provide the information of the ratio of detrital carbonate to biogenic carbonate. But some offsets exist, like the sole peak at 366.15 m in the curve of ratio Ca/Sr. This is probably resulted from the preference of Sr to be incorporated into aragonite. The low value of Ca/Sr in the upper part is obviously due to the depletion of $CaCO_3$, and thus is not informative for detrital carbonate determination.

As productivity proxies, Ba, Ca and Sr indeed reveal the remarkably high values (e.g. ~ 315 m and ~ 265 m), which can be further interpreted in a paleoclimatological point of view. They also help interpret the sedimentary environment in specific intervals. But the relatively low resolution (52 samples out of ~ 180 m) cannot reveal all notable events regarding productivity, and thus should not be simply used to reconstruct the paleoclimate change or climate cycles. However, element concentrations of Fe, S, Ba, Ca and Sr provide very important information of general sedimentary environment

changes. The coring depth of ~ 280 m is serving as a division line, below which the environment has experienced quite a few reducing condition in a suboxic or anoxic under water environments (**Figure 9** and discussion above), while above which with more contact to the atmosphere (i.e. from time to time exposed). This remarkable depth can also serve as a division of marine realm (below sea level) and fluvial realm (above sea level), considering the deltaic evolution.

5.1.2 Grain Size Distribution

There are three modalities shown in the grain size distribution of the 21 samples, two single-peak modalities showing positive or negative skewness, and one double-peak modality only for Sample 5 (see Results chapter; **Figure 7, 8**). For the single-peak modalities in the grain size distribution, skewness is one of the important descriptive statistical parameters, which is used to determine the normality or symmetry of the distribution (López, 2017). In general, turbidity flows tend to induce a negatively skewed distribution, while tsunami and torrential flows bring a positively skewed or multimodal distribution (López, 2017). In fluvial system, sorting process plays an important role on the material transportation of different grain size. Coarser grains are prone to settle sooner than finer grains, and only in faster flow and/or as part of larger discharge pulses can the coarser grains be transported further downstream. Therefore, the upstream area in a single fluvial system preferentially gives away the finer fraction of the materials, whereas the according downstream area first receives the finer grains. In other words, we can expect a more positively skewed grain size distribution in the upstream area than in the downstream area.

Figure 8 shows a very clear pattern of the skewness changes throughout the core. The depth ~ 260 m is an division, below which all the single-peak samples show negative or weak negative skewness, while the samples from the upper part mainly show positive skewness. This means the sorting process was functioning differently in the lower and upper part of the core. Negative skewness in the lower part indicates the locality of the core was in the relatively downstream area (e.g. marine or onshore area), which acted as a ‘receiver’ that received the fine grains transported here. Then the sedimentary environment has changed to a more upstream area, which was in a role of a ‘giver’ that gave away the fine grains. This is in support of the deltaic evolution in the Early Pleistocene, and the sedimentary environment might transit from marine phase to lowland phase around the depth 260 m.

Sample 5 was taken from a sub-tidal formation, which presents thin alternations of coarser and finer depositions. This leads to the double-peak curve in the grain size distribution, because the tidal cyclicity made high energy (thin current ripples in silt and fine sand) and low energy (mud drapes of clay and silt) alternate. During flood and ebb, the tidal flows were responsible for predominantly depositing the coarser sediments (coarser peak). The still stands between each tidal flow (slack water at high stands and low stands) were responsible for depositing the finer sediments (finer peak). As all the 21 samples were intentionally taken from sand lithology, we only have one sample showing the double-peak modality. But there are of course more places in the core where the sample might show this pattern, especially in the tidal formation intervals.

5.2 Sedimentary Environment Changes

The very detailed lithological and sedimentological logging gives us the opportunity to estimate the water depth, and the larger context of an interval can help us determine the relative water depth changes. Pictures of shell debris, bioturbation, peat clasts/layers and other observations that help interpret the water depth and sedimentary environment are shown in **Appendix 1**. **Figure 5d** shows the estimated water depth changes based on the detailed lithological and sedimentological logging, where the water depths are characterized as relatively deep, shallow, very shallow and supratidal. Note that the exact depth values shown in the figure are imprecise, but the relative water depth changes and the trending are more of inference. At some certain depths (e.g. 302 m and 288 m), the water depth inference was cross-checked with palynological results from the study of Krom (2020). Above 270 m, the characteristic of lithology has changed from diverse lithology with finer grains dominant to basically single lithology of massive sand, and the sedimentary environment is hence interpreted as fluvial phase. **Figure 5e** shows the estimated distance from the core to the coast line, where the characteristics are determined as inundation, shore/beach/marsh, proximal floodplain and distal floodplain. The interpretation is also based on the detailed logging and the interval context. Terrestrial/Marine ratio (T/M ratio) developed by Krom (2020) also helped the cross-verification of the interpretation (e.g. 265 m). For the interval 220 – 230 m which shows intensive and abrupt lithology changes, estimation of the environment with a higher resolution was made (**Figure 5f**). Following are the lithological and sedimentological characteristics in each interval.

5.2.1 Marine Environment and Water Depth Changes (384 – 332 m)

384 – 370 m

Diverse lithologies from clay to fine sand, and the top interval 373 – 370 m is mainly pure clay. The color is basically described as light grey and grey. A lot of bioturbations and some shell debris are found at multiple levels within this interval (**Appendix 1: Figure 1.1 - 1.3**). The water depth is regarded to represent the deepest environment compared to all higher parts of this core and is estimated to have fluctuated between 40 – 50 m. This interval is estimated to span more than 100 kyr (discussed in Chapter 6.3), and the water depth fluctuation is thus to be explained by the sea level change in accordance with the several 41-kyr glacial-interglacial cycles. The value of 40 – 50 m is regarded as an average situation over this time interval, and the detailed fluctuation is not presented.

The geochemistry of the 376.87 m sample, which consists of clay and silty sand, shows very high values of both S and Fe indicating a strong reducing environment. The sample also shows a modest peaking of Ca and Sr concentrations, which might denote a more active productivity than the other depths in this interval. The other samples for geochemistry analysis in this interval are all from coarser lithology, and are not simultaneously enriched in S and Fe. These samples are still assumed to be formed in a reducing environment, but it gives an idea that the strong reducing environment might be correlated with finer deposition.

370 – 355 m

This interval basically consists of all sand, with only the sub-intervals around 360 m and 361.38 – 361.75 m showing thin alternations of sand and silt. The color of the sand is described as light brownish grey and greyish brown. At 368.05 m there is a very thin layer of organic rich clay, which is black. Considering the relatively deep water environment of the interval below (and also that above), this sandy interval should still be in the marine phase. The water depth attributed to it is relatively shallower than that below, especially for the sub-intervals with alternations of fine and coarse grains, and has been put at 30 – 35 m. This is the most sandy interval in the marine interval of this core: the thickest bed in the log (**Figure 5a**) which has a continuous sand deposition for more than 7 meters. Coarser-grained sedimentation here could mark a larger volume of sediment deliver, which is then responsible for the shallowing of the sea. Switch of channels in delta plain nearby and/or modest sea level fall could also be

possible reasons of the shallowing. Similar to the previous interval, this interval is estimated to span more than 100 kyr, and the value of water depth (30 – 35 m) is a long-term average situation in this interval.

The sample from 366.15 m shows very high value of the ratio Ca/Sr (see also Chapter 5.1.1). As the peak does not coincide with other terrigenous-indicating elements (e.g. K, Fe), it cannot be interpreted as high terrigenous input. Sr is more prone to be associated in aragonite than in calcite, and this might be the reason for the relatively high Ca but low Sr. The high value of the ratio might be induced by foraminifera enriched, which generally contains calcite and only occasionally aragonite (Gooday, 2002).

355 – 339 m

This interval contains diverse lithologies from clay to fine sand. But unlike the lowest interval, we can observe clear alternations of sand dominant sub-intervals (~ 30 cm) and clay dominant sub-intervals (~ 10 cm). At least 15 alternations of sand and clay were found. Note that the recovery of this interval is relatively low (~ 60%), so we are likely to lose some information. The sand fraction color is mostly grey, and the clay fraction is dark grey and very dark grey. Some of the clay-dominant subintervals are presenting as pure clay, while others contain thin silt and sandy layers (likely subtidal). The water depth in this interval is also estimated as 30 – 35 m (average situation over more than 100 kyr), but it might experience frequent water depth change within the interval, because the clay dominant subintervals might be induced by the sea level drop (e.g. 41-kyr sea level oscillations, but not responsible for all clay subintervals) and/or a more slack water condition. It is also worth mentioning that there are quite a few organic rich layers in this interval (e.g. at 343.1 m and 342 m; **Appendix 1: Figure 1.5**). These organic materials might be washed from the land nearby, which confirms a shallowing trend since the last two intervals.

339 – 332 m

This interval also contains all kinds of grain size from clay to fine sand. Some non-horizontal beds of clay/organic rich layers are presented (e.g. **Appendix 1: Figure 1.6**). It looks like the continuous and extensional part of the interval just below, but we cannot observe the clear pattern of clay and sand anymore. Instead, the materials of different grain size tend to be homogeneously mixed up, or present in very thin alternations of

clay and silt/sand. The color of this interval is described as grey. Considering more thin alternations than the interval below and large stacks of tidal formation above, the water depth of this interval should be shallower than below, and showing a now rapidly shallowing-upwards pattern. The water depth is thus estimated to change from 30 m to 10 m over ~ 50 kyr.

5.2.2 Deltaic Environment and Tidal Formation (332 – 271 m)

332 – 314 m

This is the first stack of tidal formation in this core, which contains continuous thin alternations of clay and sand (or silt). So the depth 332 m also marks that the sedimentation steps into a deltaic environment, the transitional phase to the fluvial environment. The color of this interval alternates from light grey to dark grey, with the finer lithology darker and coarser lithology lighter. This stack of tidal formation can be further divided into three sub-intervals. 332 – 330 m is clay dominant tidal formation, and 330 – 326.75 m is sand dominant tidal formation. Some bioturbations can be found within these two subintervals (**Appendix 1: Figure 1.7**). 326.75 – 320.35 m is the sub-interval with alternations of clay and silt (clay dominant), and it also contains a lot of shell fragments (**Appendix 1: Figure 1.8**). There is a 4-meter unrecovered interval above the stack of tidal formation (320.35 – 315.6 m), and then a 15-cm silt interval and a half-meter fine sand interval, also containing a lot of shell fragments. In general, the water depth of this interval shows a shallower-upwards pattern, up to the fine sand interval, which is interpreted as beach sand. Therefore, the estimated water depth is changed from 10 m to 0 m. Because of the tide-induced deposition, the sedimentation rate in this interval was much higher than that in the marine/pro-deltaic phase. The estimated value of water depth is thus a shorter-time average. However, the dominant lithology of the tidal formation has changed from clay to sand and back to clay, which indicates the water depth might also experience fluctuation (e.g. deepening in the second clay dominant sub-interval). This can be explained by one full MIS cycle (41-kyr). We cannot know what happened in the 4-meter unrecovered interval, which might be more complicated than a simple shoaling pattern, and thus could cover one or two more MIS cycles.

Geochemical analysis reveals some interesting signals in this interval. Samples from 325.3 m and 320.75 m show high value of S and Fe, indicating the reducing condition. Like the sample from 376.87 m, these two samples are also from the finer

lithology, which is the clay dominant tidal formation in this case. Samples at 320.75 m and at 314.77 m (on either side of the unrecovered interval) show high values of Ca and Sr. The former is from clay dominant tidal formation, while the latter is from fine sand lithology. But visible shell fragments can be easily observed from both the depths, which induce the high values of productivity elements.

314 – 301 m

The end part of the previous interval is interpreted as beach sand (i.e. 0 m of water depth), but right above that, there goes the second stack of tidal formation. This indicates the beach sand below experienced quick drowning of 10 – 15 meters of water, which could be explained by a MIS cycle change from even to odd number (i.e. sea level rise). This interval also contains continuous thin alternations of clay and sand (or silt), and the color ranges from light grey to very dark grey, with some fine sand fractions showing a bit of brown. A half-meter silt interval (307 – 307.5 m) divides the interval into two half, with the lower half showing mm-scale alternations of clay and silt (medium difference in tidal energy; relatively deepened water; e.g. **Appendix 1: Figure 1.9**), and the upper half showing alternations of clay and sand (strong difference in tidal energy; shallowing water). The top part of this interval is a 1.5-meter fine sand interval, which can be interpreted as beach sand. Unlike the top part of the previous interval, no shell fragments are spotted in here. Given that this interval is right above a beach sand section, the water depth should have been deepened at the beginning of this interval to start up a new stack of tidal formation. Similarly, this interval could experience another shoaling process to the beach sand deposition at top. Therefore, the water depth is estimated to change from 15 m to 0 m (short-time average and trend of shallowing). Considering this interval is also about 15-meter thick (with a little compaction), it supports that the sedimentation since the interval below is continuous.

301 – 283 m

This interval is much more complicated to interpret than those below, due to diverse lithologies and irregular deposition and two non-recovery intervals. The lower part of this interval (301 – 293 m) is clay dominant with sand influence, and mainly present in greyish brown or brown color. The recovery is only about 50% here. It is very hard to find out the connection between each separated sub-intervals and to make estimations on the water depth. The upper part (293 – 283 m) mainly consists of fine

sand, with the color light brownish grey and light grey. Some shell fragments are found around 292 m. This sand section looks similar to the deep sea sand interval at 370 – 355 m. Considering a larger context of this interval, where it is following a stack of tidal formation and also followed by one, the sand section here might be under a relatively deep water environment. However, not much information regarding water depth changes/fluctuations can be revealed.

The sample from 288.4 m is remarkable as it shows strikingly high values of heavy mineral content, Ti and Zr. The sample is from fine sand lithology, where it clearly shows two parallel black sand layers. This might be due to some extreme events, such as volcanic eruption, that can lead to heavy mineral concentration.

283 – 271 m

This is another typical stack of tidal formation, which is also the last stack and the one with the best continuity of the thin alternations. Similar water depth interpretations as for the earlier intervals 332 – 314 m and 314 – 301 m apply. Within the interval, the depositions change from clay dominant alternations to sand dominant alternations, and the color changes from dark greyish brown to light greyish brown accordingly. Around 277 m, there are some depths only contain sand, but the alternations of finer and coarser materials continue well in general. Some bioturbations are observed around 282 m. All the evidences support a shallower-upwards pattern, and the water depth is thus estimated to change from 20 m to 0 m.

Starting from this interval, co-variations between some elements change. S is disconnected with Fe, and builds up a new correlation with Ba. Sr stops the co-variation with Ca, but also starts to co-vary with Ba. As mentioned previously, this marks that the sedimentary environment is more exposed to the atmosphere from here on.

5.2.3 Lowland/Fluvial Environment (271 – 195 m)

271 – 256 m

Above 271 m depth, the ‘tidal’ alternations of finer and coarser micro-beds no longer occur, and the dominant lithology becomes basically all sand (the interval 225 – 220 m is an exception).

A combination of properties indicates that the sedimentation regime has changed to that of a fluvially dominated environment. The recovery of this interval (271 – 256 m) is still reasonable (worse than the tidal intervals below, but better compared to the other

intervals further above). The first half of this interval (271 – 261 m) is all medium-grained sand, presenting in brown, pale brown or very pale brown. Very few displaced peat clasts can be found around 268 m. This part is interpreted as the product of river channels in normal deltaic floodplain. Considering the position of the Petten Borehole in the southern North Sea Basin and given that it is the onset of the fluvial phase deposition in the sequence description, the coast line will have been position nearby the core locality. The second half of this interval (261 – 256 m) interestingly contains a lot of peat layers, and more than 80% organics of the core is existing in this sub-interval. The thickness of these black peat layers are from 1 cm up to 15 cm. The sand fraction in this sub-interval, in the color of grey or light brownish grey, is mostly fine sand and silty sand. It is obviously that the upper half contains much finer grains than the lower half. Both the peat layers and finer sediments indicate that the core during the upper half was getting closer to the marine than that during the lower half. Thick peat layers likely are induced by inundation and high productivity, which could be the marsh environment.

Sample from 264.55 m shows the highest S, Ba and Sr of all 52 samples. This sample was taken from a fine sand section, which is right above a 3-meter unrecovered interval. As all these three elements point to marine productivity, some of the deposits should be directly sourced from the sea. We cannot know how exactly the sedimentary environment changed during the 3-meter unrecovered interval, but it is possible that the coast line has transgressed very close to the core location, whereby the wave or tide could transport the materials from the sea to here (incidentally during a storm or for a short episode of highest sea level and insufficient river sediment supply).

As for grain size distribution, two samples taken from this interval (269.02 m and 262.22 m) still show negatively skewed distribution curve. This means the sedimentary environment was still at a relatively downstream area. However, since the environment has now changed to floodplain, the sediments are brought here when channels pass by, and the sedimentation rate is thus much lower than that in littoral/delta front phase. Also, water depth no longer apply to this interval and those above, where the distance from the core location to the coast line gives the general description of environment change in the delta plain phase (**Figure 5e, 5f**).

256 – 236 m

In this interval only 50% of the sediment was recovered. It consists in great

majority of medium sand, with some parts showing fine/silty sand and coarse sand. The color is described as light brownish grey and greyish brown. Some peat clasts are found around 244 m. Some fine gravels and rock fragments are recovered around 236.5 m (**Appendix 1: Figure 1.13**), but with little context information, it cannot be interpreted precisely. It is possible that the gravels and rocks were brought by glacial movements. The characteristic sedimentary environment for this interval is interpreted as floodplain. Changes in dominant grain size might be induced by discharge changes and/or changes of distance to the coast line.

Samples for grain size analysis start to show positive skewness in the distribution curves (**Figure 7**) from this interval upwards (**Figure 8**). All three samples taken from this interval (255.83 m, 250.22 m and 240.88 m) contain more coarser fractions than finer fractions. These results support the deltaic evolution, in which the core was gradually changing to upstream situation: coarser grains tend to settle sooner than the intervals below, and finer grains are then the majority that can be transported further downstream.

236 – 219 m

There is a 5-meter unrecovered interval above the rock fragments mentioned above, so the recovered materials of this interval actually start from 231.5 m. The typical characteristic of this interval is the straightforward pattern of sand (~ 1 m) / clay (~ 30 cm) alternation. At least 5 para-cycles of this alternation were registered. The sand sections contain medium sand and are light brownish grey at base, but gradually change to fine sand and grey or dark grey at top. Some peat clasts can be found around 231.5 m. The lower clay sections contain quite a lot of peat clasts or layers, within which thin alternations with sand can also be found. However, the upper clay sections are mostly clean and pure clay. The color of clay sections also changes from black to dark grey or grey. Considering the lithology changes frequently and abruptly in this interval, more observations were conducted to make the sedimentary environment change with a higher resolution (**Figure 5f**). Similar to the other intervals in this phase (271 – 236 m), the sand sections here are interpreted as modest size fluvial channels operating in the delta floodplain (branches of larger river channels; delta distributaries and crevasse-like systems). The lower clay sections with peat would be flood basin marsh environments in the delta plain, where the tide might also play a role. Equivalent environments are described for the Holocene high stand Rhine-

Meuse delta in the western Netherlands (Berendsen and Stouthamer, 2000; De Haas et al., 2018) and for Last Glacial falling stage (e.g. Hijma et al., 2012; Cohen et al., 2014). The fluvial floodplain environments in the south of the Netherlands described by Westerhoff (2009) would be inland equivalents, and the floodplains at Petten would be quite far downstream in the delta plain. The upper pure clay sections, indicate a more slack water and lower productivity environment, which could be by the shore or be inundated. Palynology-based T/M ratio developed by Krom (2020) in the parallel thesis indicates a value of 0.9 for both the samples at 222.45 m and 221.2 m, compared to a value of 1 (terrestrial) for most of the samples from 250 m above. This results also support the explanation. The sand and clay alternation in this interval is attributed to fluvial dynamics, which can cause the change of water depth and position to coast line at the location of Petten Borehole, and further induce the different environments of fluvial channels and flood basin marsh. The overall trend in this interval, however, can be attributed to sea level rise in a MIS cycle: deeper water condition in the upper part leads to stronger oxidation, and thus the upper clay sections with more greyish color and less organic content. The finer-grained sand in the upper sand sections can also support it.

There are three samples taken for grain size analysis in this interval (230.7 m, 222.7 m and 220.75 m; **Figure 7**). The sample from 222.7 m shows a negative skewness (i.e. still water trapping of full sediment influx), whereas the other two show a positive skewness (i.e. channelized transport, sorting of bed load and through-pass of finer fractions). This also indicates that the sedimentary environment changes frequently and greatly in this interval, that the core was changing many times among relatively upstream area, relatively downstream area and even inundation.

219 – 195 m

This is the topmost interval in the study section of this core, and the recovery condition here is the lowest in the whole study (less than 10%). The recovered materials are almost all medium to coarse sand, except a 15-cm clay layer around 217 m. The color is described as light brownish grey and pale brown, which also makes it one of the most brownish intervals. This interval could be interpreted as the step into a more steady floodplain environment, but given the very pool recovery condition, we cannot make sure. The sample from 201.88 m, which shows a weak negative skewness on grain size distribution curve (**Figure 7**), also makes the interpretation

more cryptic.

5.2.4 Interpretation Summary

To sum up, the study section of this core (384 – 195 m) is divided into 3 parts in terms of the sedimentary environment changes, the marine phase deposition (384 – 332 m), the transition phase deposition (332 – 271 m) and the fluvial phase deposition (271 – 195 m) (**Figure 5**). Characteristic lithology has gradually changed from a more diverse composition at base to simple massive sand at top. The water depth interpretation reproduces an overall shallowing-upwards accordingly, with superimposed water depth variations that likely correlate to MIS-associated sea level variations.

In the marine/pro-deltaic phase, the sedimentation experienced suboxic and anoxic environments. Also, it is worth mentioning that these signals (i.e. high Fe and high S) only appear in the samples from finer lithologies, like clay, silt or silty sand. Even with a relatively lower resolution of element analysis, we could infer that slack water condition, which is responsible for finer depositions, explains the geochemically suggested suboxic to anoxic sea-floor environment.

In the littoral/delta front phase, the representative depositions are the three stacks of tidal formation. Each of the stack shows a shoaling process, which reveals how water depth change has an impact on the deposition during the transition phase from marine to lowland environment. Note that due to the poor recovery condition, more stacks of tidal formation might also exist. So we might have lost some information of the sea level fluctuations during this phase, but have recorded at least three MIS cycles.

In general, the fluvial/delta plain phase in this core is not very steady, which can be proved by a lot of peat and clay deposits, and occasionally high values in marine productivity proxies. So a certain part of the deposits in this phase might be still directly sourced from the sea.

5.3 Sediment Hiatus and Extreme Events

Alongside the lithological and sedimentological logging, we also noted down the contacts that might be induced by marked erosion events. These contacts are usually presenting in abrupt lithology change. Some erosion events might be simply resulted from sea level fluctuations, while the others might be in a much larger scale, such as open field erosion. Spiky grass peaks in the palynological curves from the parallel study also support the potential erosion events in the fluvial/delta plain phase

deposition (Krom, 2020). Pictures of the contacts potentially responsible for erosion events in this core can be found in **Appendix 2**. Following are the interpretations for some typical contacts. All the contacts found in this core are shown in **Figure 10**, where the depths are also indicated. Overall speaking, the erosion events occurred from 330 m upwards in the deltaic and fluvial environment. Also, due to the low recovery condition in both transition and fluvial phase deposition, we might have lost a lot of information. Contacts responsible for major erosion events are thus difficult to identify.

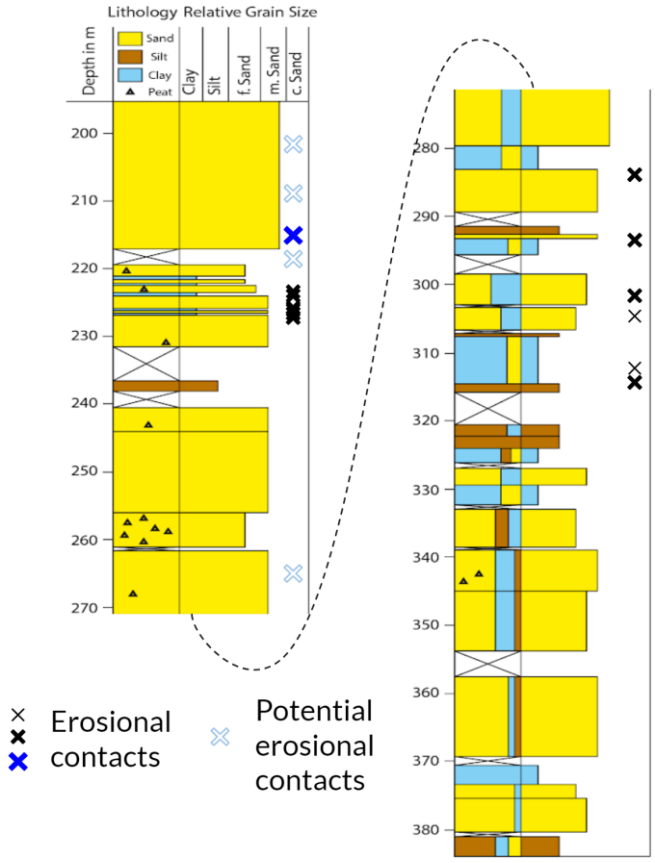

Figure 10 *Contacts found in the core that are potentially responsible for erosion events and sediment hiatus. Black crosses (thin and thick) stand for small scale erosion events. Blue crosses (solid and hollow) stand for large scale erosion events. The blue hollow crosses are at the inferred depths which were not recovered, and the depths are thus not accurate.*

Contact at 314.5 m (**Appendix 2: Figure 2.1**) shows an abrupt change from fine sand to clay. This contact is at the top of the first stack of tidal formation. The sample taken right below the contact (from the fine sand fraction) reveals very high Ca and Sr, and a lot of shell fragments can be found here as well. As mentioned previously, the

sand here is interpreted as beach sand. The clay section above contains alternations with thin sand layers, which is believed to be formed in a sub-tidal environment. Therefore, the water depth here changes from ~ 0 m to ~ 15 m, which is due to sea level rise and/or geological subsidence. This contact hence could have recorded a small erosion event, incorporating beach sands and displacing them to the core locality, possibly resulting from a major storm (changing the coast line) or from a phase of marine transgression (phase of relative sea-level rise).

The contact at 302.7 m (**Appendix 2: Figure 2.2**) is in the top part of the second stack of tidal formation. Unlike the previous contact, this one shows the change from clay to fine sand. The clay section here contains the thin alternations with sand, which is thought to be formed in the intertidal environment, and the fine sand section here is regarded as river delivered. Potentially, it was a sea level drop that caused the lithological change and the contact. Discharge in river channels increased as the sea level fell and the delta plain evolved from high stand trapping environment to low stand through pass environment (e.g. Westerhoff, 2009: Fig. 6.10). Such effective discharge increase might have flushed away the top part of the tidal formation as well as the early fluvial deposits. This also explains why the sand section does not contain as many shell fragments as the sand section around 315 m does, because the lower part of the beach sand deposits might be eroded this time. The contact at 293.05 m (**Appendix 2: Figure 2.3**) shows very similar pattern as contact at 302.7 m, which is also an abrupt change from clay (alternations with sand) to fine sand. The story of erosion could be similar.

At the base of the third stack of tidal formation, there is a contact (282.7 m; **Appendix 2: Figure 2.4**) showing the abrupt change from pure clay to silt. This is also a change from finer to coarser lithology, but given the both side of this contact are below the water level, the scenario could be different. Storm could be responsible for this contact, which could rework the deposition and only the relatively coarser grains were re-deposited again.

The interval 228 – 220 m includes the regular pattern of sand and clay (**Appendix 2: Figure 2.5**), and each time when the lithology changes, erosion could occur. The contacts of different lithologies in this interval do not keep the same appearance, which are more abrupt in the lower part, and more gradual in the upper part. The sand/clay pattern was induced by fluvial dynamics, but none of these contacts are responsible for very large scale erosion events.

The contact at 216.9 m (**Appendix 2: Figure 2.6**) is found in the very poorly recovered interval, which has very little context information. The contact shows the change from pure clay to medium sand, which is the one with the largest grain size difference found in this core. Also given the fluvial environment, this might be responsible for a very large erosion event. But the poor recovery condition limits the further interpretation.

Besides all the contacts found in the core, some other erosion events might occur in the unrecovered intervals that we cannot see. But some signals in recovered materials could lead us to guess where the potential sediment hiatus are. **Figure 2.7** in **Appendix 2** shows the 3-meter unrecovered interval, which locates in the beginning of the fluvial phase deposition. Sample taken right above the interval reveals the highest Sr, S and Ba, which indicates parts of the deposits might be directly sourced from the sea. It is then very possible that the sedimentary changed severely during the unrecovered interval, including experiencing large scale erosion events. Also, from 200 m above, the recovery condition is less than 10%, which also remains the possibility of major erosion events.

5.4 Provenance Changes

Provenance of the sediments can be determined from heavy mineral associations. Besides, the correlations between heavy mineral content and elements that are mainly associated with certain heavy minerals (e.g. Ti and Zr in rutile/anatase and zircon) can also contain valuable information regarding provenance changes. As mentioned in the Geochemistry chapter, heavy mineral content has good correlations with Ti and Zr. Also, the co-variations remain in phase throughout the core. This result can infer that Ti and Zr do exist in the heavy minerals, and the provenance of the sediments does not change significantly in the study section of the core. If the provenance of the sediments changes to another source, which assumably contains different composition of heavy minerals, we should expect worse correlations between heavy mineral content and Ti and Zr, or good correlations but within two separated intervals. Both Rhine and Eridanos river systems could be responsible for the sediments in the NW Netherlands in the Early Pleistocene. But Eridanos had an impact on this region earlier than Rhine (e.g. Gibbard et al., 1988; Westerhoff, 2009), and further formed the Peize Formation. Therefore, the provenance of the sediments in this core is believed to be Eridanos river system to the east, and the provenance does not change significantly in

the Early Pleistocene according to the heavy mineral and geochemical results.

5.5 Age Model

Prior to the beginning of this research, a first tentative age model of the Petten Borehole 1 was established by Houben (2019), using paleomagnetism and palynology. Since then, Krom (2020) conducted more palynological analyses in the parallel thesis to improve the age model, and also findings regarding sedimentation rates, erosion contacts and water depth fluctuations from this thesis are new information that may be utilized to iterate and improve the age model.

Krom (2020) selected 70 samples out of the study section of the core (384 – 195 m) for palynological analysis, and samples are mostly from finer lithologies (i.e. clay an silt). The palynological results in the parallel thesis do not show much difference from Houben (2019) on the estimated age of each sample, and the tie points thus remain the same. Similarly, due to the poor recovery in the upper part of the study section, no solid tie points were made. Therefore, the paleomagnetism- and palynology-based age model remains the same as the black solid line in **Figure 4**. In addition, Krom (2020) highlights the last occurrence of a dinoflagellate, *A. umbracula*, to date the stratigraphy. The last occurrence of this species is in the sample from 304.9 m, which is accredited with the age ~ 1.8 Ma, near the top of the Gelasian. However, this sample is encountered well above the presumed Olduvai 'normal polarized' time interval in the core (estimated: 322 – 355 m; Houben, 2019), which spans the age of 1.78 – 1.94 Ma. That either suggests that the 'last occurrence' level in Krom (2020) is placed too high (i.e. in a reworked level), or that the identification of the Olduvai interval in Houben (2019) is misplaced (i.e. that normal polarity interval is a pre-Olduvai one instead, and Olduvai interval should be sought around 300 m), or that the last occurrence is slightly later than generally accredited.

Sedimentation rates and water depths estimated in the sedimentological study can help improve and cross-verify the palynology- and paleomagnetism-based age model. Water depths in marine/pro-deltaic phase are estimated to change from 50 m to 10 m through time, with several fluctuations but a general trend of shallowing (**Figure 5**). However, there are two intervals (384 – 370 m and 370 – 340 m) of which the water depths can be regarded as long-term steady. Water depths of 384 – 370 m are fluctuated between 40 – 50 m and water depths of 370 – 340 m around 30 m. We can thus infer that the sedimentation rates within these two intervals were basically in

accordance with the contemporary subsidence rates, which is approximately 100 m/Ma (Kooi et al., 1991). The strikingly fast shallowing of the water depth around 370 m (**Figure 5**) is then an indicator of temporary high sedimentation rate, which outruns the subsidence rate. This slow-fast-slow pattern is also presented in **Figure 4**, in spite of a little offset, which proves a cross-verification of palynology/paleomagnetism and sedimentology. As the delta front passed by in the littoral phase, we can expect a much higher sedimentation rate than that in the marine/pro-deltaic phase: three stacks of tidal formation can be formed in a very short time. Also, more sediment input can reinforce the subsidence, and thus a higher subsidence rate. Plus the shallowing water depth, it leads to an estimation of even higher sedimentation rate. **Figure 4** again supports the acceleration of sedimentation rate from 357 m. However, marked erosional contacts and frequent unrecovered intervals are found from this phase, which causes potential hiatus in the sedimentary history and loss of some sedimentary information. It means the short-term sedimentation rate (e.g. in each stack of tidal formation) is much higher than the long-term sedimentation rate (in the whole interval of the littoral/delta front phase). This can explain why **Figure 4** does not show an even higher sedimentation rate from 357 m, rather it is similar to that around 370 m: because the palynological and paleomagnetic tie points are in a very low resolution above 357 m, and short-term sedimentation rates hence cannot be revealed in the curve. Similar to palynology and paleomagnetism study of the age model, the low recovery condition in the fluvial/delta plain phase restricts the detailed discussion of sedimentation rate in the sedimentological point of view. More about subsidence rate and sedimentation rate is discussed in Chapter 6.3.

6. Discussion

6.1 Eridanos-Rhine Delta Development during the Early Pleistocene

As introduced in the Background chapter, the southern North Sea Basin was fed by several river systems during the Early Pleistocene (Gibbard et al., 1988), of which Eridanos and Rhine-Meuse river systems drained most part of the Netherlands, and could be responsible for the sediments in the northwestern Netherlands (Rijsdijk et al., 2005; Westerhoff, 2009). The Eridanos river system was formed during Late Oligocene or Early Miocene, and it kept evolving westwards through the northwestern Europe

since then (Overeem et al., 2001). During the Late Pliocene, the depocenter of the Eridanos river system shifted southwards significantly, and southwards progradation was also mapped in the northeastern Netherlands (Overeem et al., 2001). This movement greatly helped the system drain most of the Netherlands later in the Pleistocene. In the middle Early Pleistocene, when the southeast of the North Sea Basin has been infilled from marine to lowland, the depocenter of the Eridanos river system received significantly more sediments from the south (Overeem et al., 2001). Over the same Late Pliocene to Early Pleistocene time period, the Rhine-Meuse river system expanded northwards and westwards outwards from the Lower Rhine Embayment in the southeastern Netherlands (Gibbard et al., 1988; Westerhoff, 2009; Kooi et al., 1991). The expansions of these two river systems in this time period are seen as evolving independently. As the sphere of influence of Eridanos moved southwards and Rhine-Meuse kept evolving northwards, they eventually joined in the middle Netherlands during Waalian Stage (Overeem et al., 2001), and built up the huge converged delta system. The contemporary offshore formation is known as the Yarmouth Roads Formation (e.g. Funnell, 1996; Rijsdijk et al., 2005).

This study is based on the core (Petten Borehole 1) from the northwestern Netherlands, which is believed to cover the whole Pleistocene. According to all the observations and analyses, the study section of this core (195 – 384 m) does show a shallowing-upwards pattern, transiting from marine phase deposition to fluvial phase deposition – in other words: an expanding delta front migrated across the core location. This confirms the general insights on the delta progradation in this area during the Early Pleistocene. Also, from the provenance study, the sediments of the core are convincingly sourced from Eridanos river system (at least in part; see below). Therefore, the shallowing pattern of the core corresponds to the near final stages of southwestward progradation of Eridanos delta front. The direction of the progradation is mainly thought to be westwards, but a northwards to northwestwards progradation is also possible, as Eridanos has evolved southwards since the Late Pliocene.

Besides, it is very interesting to find out whether also the Rhine-Meuse river system had an impact on the sediments in this core. The Rhine-Meuse river system in the Early Pleistocene was of a relatively smaller scale than the Eridanos, and its delta plain only merged with Eridanos system when that was finishing its major progradation across the northern Netherlands. From previous core studies of the same timeframe (see also Chapter 2.3), Borehole De Meern, to the southeast of this core, shows

interdigitation of Eridanos sediments (Peize Formation) and Rhine-Meuse (Waalre Formation) sediments, while Borehole Hippolytushoef, to the northeast of this core, exclusively shows Eridanos sediments. Apparently, areas that far north in the Netherlands were not yet affected by the Rhine-Meuse river system in the Early Pleistocene. According to Westerhoff (2009, *Figure 6.9*), Petten Borehole 1 is located at the furthermost border that the Early Pleistocene Rhine-Meuse delta plain occupied in the Early Pleistocene. We might expect some signals of Rhine-Meuse in the upper half of our study section in this core. Also, palynological composition from the lower half of the study section suggests some contributions of species sourced from warmer or southern areas. So the influence of Rhine-Meuse can neither be ruled out in the lower part (marine/pro-deltaic phase). However, the very poor recovery condition restricts the further analyses, and the mystery of Rhine-Meuse then remains unraveled. Some assumptions regarding Rhine-Meuse can thus be made: it could well be that a real change from Peize Formation to Waalre Formation happens higher up than 200 m in this core. Considering the Eridanos delta front passing through the northern Netherlands in the middle part of the study section, it is also possible that the very base and the very top of the section have a bit more influence of Rhine-Meuse than the middle part. But it is still clear that Eridanos delta was evolving and feeding the northwestern Europe (including the region of Petten Borehole 1) independently, and not until a later point (which cannot be determined in this study) does Rhine-Meuse have the possibility to join the delta evolution.

6.2 Presumed Glacial and Interglacial Parts of the Succession

The Earth gradually stepped into a glacial-interglacial alternating world, ruled by 41-kyr cycles during the Pliocene, and climate/sea-level cycles of that length were clearly established during the Early Pleistocene. This 41-kyr glacial-interglacial alternation lasted throughout the Early Pleistocene (**Figure 3**). According to the MIS standards (Lisiecki and Raymo, 2005), approximately 40 cycles are there in the Early Pleistocene.

In northwest Europe (notably the Netherlands and the North Sea Basin), people have been working in the last century on the palynological zones to subdivide the Pleistocene, and Zagwijn (1985) established the modified chronostratigraphic subdivisions of the Pleistocene in the Netherlands. According to Zagwijn (1985), the Early Pleistocene in the Netherlands went through Pre-Tiglian (cold), Tiglian (warm), Eburonian (cold), Waalian (warm), Menapian (cold), Bavelian (warm). These

chronostratigraphic units are called Regional Stages and Substages (e.g. **Figure 3**). Each sub-stage contains several 41-kyr cycles, and the cold (warm) periods also include warm (cold) subintervals (**Figure 11**). Generally speaking, these sub-stages aim to characterize the Pleistocene in terms of temperature in a larger time-scale than the 41-kyr cycles. A pollen-based July temperature is also in **Figure 11** next to the sub-stages.

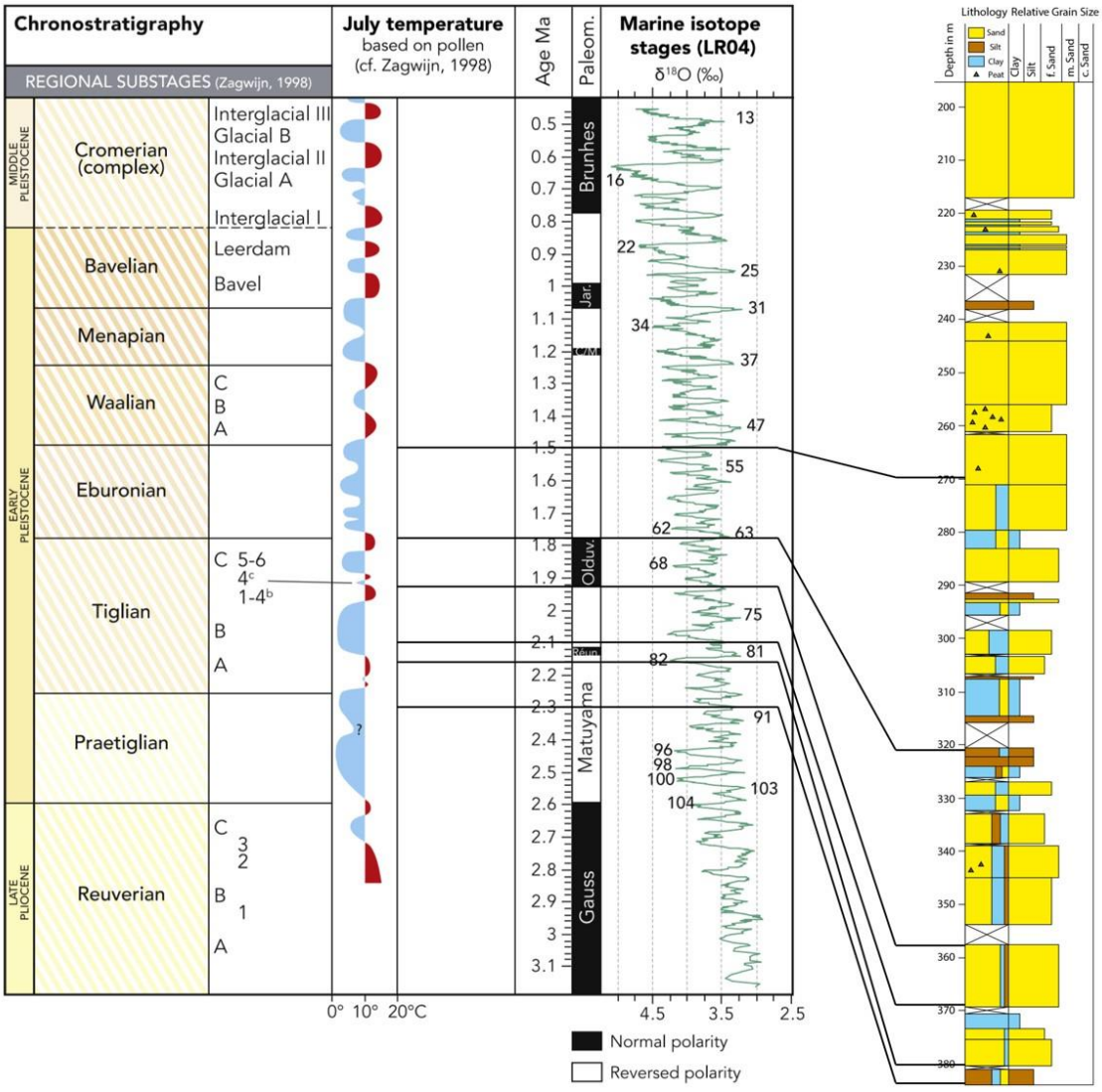

Figure 11 *Palynology-based chronostratigraphic subdivision of the Early Pleistocene in the Netherlands, with a pollen-based temperature curve (Zagwijn, 1998) and the paleomagnetic record (after Westerhoff et al., 2020: Figure 1). Black solid lines correlate the sedimentary record in this study to the chronostratigraphy based on palynology- and paleomagnetism-based tie points (as in* ***Figure 4****).*

Since the previous paleomagnetic and palynological study provided the age-depth model, it gave us the chance to tune the lithological and sedimentological logging with the sub-stages in the Early Pleistocene (**Figure 11**). From the tuning, we can discuss which parts of the succession were formed in a colder period, and which parts in a warmer period.

Interval 384 – 370 m is correlated to late Praetiglian and Tiglian-A, where Praetigilian is thought to be a cold period, and Tiglian-A a temperate period. This interval consists of diverse lithologies, from clay to fine sand. It shares similar characteristic and appearance throughout the interval, with only the top three meters pure clay. According to the tie-points, the lower part (380 – 384 m, the more silty interval) is correlated to the late Praetiglian, and the rest to Tiglian-A. But it is also possible that the interval was all formed in a relatively temperate climate, as the tie-point at very base of the core is more assumable (could be correlated to a younger time). In the correlation, interval 380 – 370 appears to cover one and a half MIS cycle (ca. 60 kyr), while the lithology, showing a trend from fine sand to clay, seemingly presents one full cycle. This could be attributed to a weak MIS cycle (MIS 80) or a bit offset from palynology/paleomagnetism.

Interval 370 – 355 m, the most sandy interval in the marine phase deposition, is correlated to Tiglian-B, a cool period. The estimated water depth in this interval is interpreted to be shallower than the previous interval. The age-depth model here further reveals the temperature in this interval is lower than that in the previous one, so the shallowing water depth might be induced by the sea level going down (could also because of the temporary high sedimentation rate before this time interval). The regression of the sea would lead to erosions in the formed lowland and delta area, which could explain the sandy deposition in the offshore area. The correlation indicates that this interval spans approximately 4 MIS cycles (160 kyr: 2.1 – 1.94 Ma), while the sandy lithology does not present much about cyclicity. There is the possibility that the sand bed was formed within one MIS cycle, being reworked repeatedly in the following cycles, and eventually represents the full time interval.

Tiglian-C is a temperate complex sub-stage that is fairly well resolved in original type sites in the southeastern Netherlands (Zagwijn, 1986; Westerhoff, 2009). It has at least two cool intervals (Tiglian-C 4c and 6). In **Figure 11** it is correlated to the interval 355 – 320 m of the core, the interval thought to be concurrent with Olduvai event (in the preliminary age model; Houben, 2019; **Figure 4**). This sedimentary interval

contains the upper part of marine phase deposition and the first stack of tidal formation (littoral deposition). The lithology is diverse in this interval, ranging from clay to fine sand. Some sand/clay dominant patterns can be observed, which could be in accordance with the complex temperature change (and sea-level variations) during the Tiglian-C Substage. The Olduvai event spans about 160 kyr, which roughly equals to 4 MIS cycles. If the tidal formation (332 – 320 m) is attributed to the top MIS cycle, the rest part (355 – 332 m) is then correlated to 3 MIS cycles. Not much information about cyclicity can be acquired from lithology in this part, but the calculated long-term sedimentation rate (192 m/Ma) is reasonable in the last stage of pro-deltaic phase.

The Eburonian, succeeding the Tiglian, is a cold complex with at least three warm subperiods. This Stage is correlated with the interval 320 – 270 m of the core, which covers the last two stacks of the tidal formations. From the correlation, the first stack of the tidal formation might also be included within the Eburonian. The typical sedimentary characteristic in the littoral/delta front phase is the thin alternations of clay and sand, and the three separate stacks of shoaling patterns. The cold/temperate period alternations during Eburonian might be responsible for the sea level change, which further resulted in the several stacks of tidal formations: when the climate changes from cold to temperate, the rising sea level could stop the previous tide-inducing deposition. When cold conditions return and sea level falls another shoaling process can start. When it became colder, sea level was in low stand for a larger part of time making that average water depth decreased, which is indeed what was observed (Chapter 5.2). However, it is hard to exactly correlate each stack of tidal formation from the core to each cold/temperate period in Eburonian, because the recovery condition is not good enough to do so. Also, the resolution of palynological analysis is not high enough to verify these detailed correlations. According to the age model, this interval spans from 1.78 Ma to 1.5 Ma, covering ca. 7 MIS cycles. If the two stacks of tidal formations are attributed to 2 of these cycles, 5 cycles are missing. Concerning the marked erosional contacts and relatively poor recovery condition in this interval, it is possible that very few sedimentary information is preserved.

From 270 m above, the depositions are interpreted as fluvial phase. Due to the low clear palynomorphs yield from this depth above, no further tie points are determined. According to previous age estimation of the depth 200 m, it could drop in a range of 0.8 – 1.2 Ma (Houben, 2019). This means the top of the study section (i.e. ~ 195 m) could be in the Menapian or the Bavelian. But there still are some evidences

in the sedimentation that can help to correlate the core to cold/warm periods. Waalian, following Eburonian, is a warm sub-stage with one cool interval (Waalian-B), and the peat rich interval 261 – 256 m could be correlated to one of the warm intervals in Waalian. It has mentioned previously that interval 235 – 219 m shows a more greyish and less organic trending, which could be due to cooling environment. But it is hard to tell which cooling trending in the curve is responsible. If this cooling trending is the Waalian-Menapian transition (~ 1.25 Ma), the sedimentation rate here in the fluvial/delta plain is 172 m/Ma, which is a bit lower than that of littoral phase before (180 m/Ma, long-term average value). If it is correlated to the cooling environment within the Menapian (~ 1.15 Ma), the sedimentation rate here is then 123 m/Ma. Considering the potential erosion events and poor recovery condition, the rest cannot be correlated to the age model.

In general, 20% deposition in the marine phase deposition is thought to be formed during cooler period (Tiglian-B) in the interglacial complex Tiglian, and all the tidal formations in the transition phase deposition are thought to be formed in the glacial complex Eburonian. The rest in the fluvial phase deposition is hard to be interpreted as glacial or interglacial depositions based on palynology-based age model. But both glacial and interglacial depositions have their evidences in the recovered materials of the core.

6.3 Subsidence and Sedimentation Rate in the Southern North Sea Basin

A fairly high subsidence rate is a typical characteristic in the North Sea Basin during Quaternary. The subsidence rate in the North Sea Basin is estimated to be 100 m/Ma during Quaternary, in comparison with 5 m/Ma during Paleogene and Neogene (Kooi et al., 1991). Note that the estimation of subsidence rate in this region is strongly dependent on understanding of the system, and thus the values from Kooi et al. (1991) should be regarded explorative. The tectonic and isostatic subsidence (Kooi et al., 1998), together with continuous sedimentation brought by several river systems, led to the large Quaternary sediment thickness in this region. As for the Petten Borehole 1, we can use the age-depth tie points and estimated water depth to roughly calculate the subsidence rate. Using the tie point at 380.91 m, which has an estimated age of 2.16 Ma and estimated water depth of 40 m, together with a presumed sea level of –50 m, the subsidence rate since 2.16 Ma in this region is about 135 m/Ma. As we have the tie points, age-depth model, and estimated water depth curve, subsidence rate of

different intervals can also be calculated. The formula is:

$$r_{sub} = \frac{(CD_2 - CD_1) - (WD_2 - WD_1)}{EA_2 - EA_1}$$

with r_{sub} the subsidence rate, CD_1 and CD_2 the core depths of the upper and lower tie points, WD_1 and WD_2 the estimated water depths of the upper and lower tie points, and EA_1 and EA_2 the estimated ages of the upper and lower tie points. Note that this formula does not consider the eustacy, which means we use a 41-kyr cycle averaged sea level.

The results are shown in **Table 4**. Basically, we can see the subsidence rate is accelerating upwards. We do not have any tie point in the fluvial phase deposition. But even if we do, we cannot calculate the subsidence rate using the formula, because we do not have the estimated elevation (counterpart to estimated water depth in the marine/pro-deltaic and littoral/delta front phase) of the deposition.

Besides the subsidence rate, sedimentation rate is also important to discuss. Calculation of sedimentation rate is simpler than subsidence rate, because we do not have to consider water depth or eustacy. The formula for sedimentation rate of each interval is:

$$r_{sed} = \frac{CD_2 - CD_1}{EA_2 - EA_1}$$

Note that compaction is not considered in this formula. The results are also shown in **Table 4**. We should be cautious to the sedimentation rates here, because these are only the long-term average rates in each interval, and if erosion events occurred in the interval, the actual sedimentation rate could be much higher. In **Table 4**, we only calculated the sedimentation rates for the marine phase and transition phase intervals, where the erosion events are not likely to occur frequently. But we should also bear in mind that erosion is observed in this core from 330 m upwards. Three intervals in the table show the sedimentation rate higher than 185 m/Ma, while the interval 369 – 357.12 m only has a rate of 74.25 m/Ma. This is in accordance with the climate-depth correlations shown in **Figure 11**, where this interval is correlated to a cooler period. The relatively lower temperature might induce a smaller discharge and slower runoff, and thus further slows down the sedimentation rate. Interestingly, interval 321.7 – 269.5 m is also correlated to a cooler period, but showing a much higher sedimentation rate. This is because this interval consists of stacks of tidal formations, which could be largely formed within a short time. Plus the ongoing subsidence of the basin, accommodation for depositions remained at a high level in this interval. Due to the

large-scale erosion events and poor recovery condition in the fluvial phase deposition, it is very hard to calculate or estimate sedimentation rate above 270 m.

Table 4. Calculated subsidence rates and sedimentation rates of 4 marine and littoral intervals below 270 m (380.91 – 269.5 m), using selected palynology- and paleomagnetism-based age-depth tie points.

Core depth (m)	Estimated water depth (m)	Estimated age (Ma)	Subsidence rate (m/Ma)	Sedimentation rate (m/Ma)
269.5	0	1.5		
			168.57	186.43
321.7	5	1.78		
			65.13	221.38
357.12	30	1.94		
			74.25	74.25
369	30	2.1		
			31.83	198.5
380.91	40	2.16		

7. Conclusion

The lower half of the Petten Borehole 1 has been studied on sedimentological and palynological history of the Early Pleistocene in the southern North Sea Basin by two parallel MSc theses, and this study has been focused on lithology and sedimentology of the core. Satisfying the aims of the research, sedimentary environment changes, provenance of the sediments and hiatus in the sedimentary history are revealed.

The study section of the core (384 – 195 m) shows the obvious pattern of a transition from marine phase deposition to fluvial phase deposition. The core is thus divided into three parts, the marine/pro-deltaic phase (384 – 332 m), the littoral/delta front phase (332 – 271 m) and the fluvial/delta plain phase (271 – 195 m). Marine/pro-deltaic phase deposition basically consists of silty sand and clay. It shows a shallowing-upwards pattern in terms of the estimated water depth, and it was getting closer to the coast. Geochemical data has revealed that this interval experienced suboxic and

anoxic environment. Littoral/delta front phase creates a more complicated deposition than the other two phases. There are at least three stacks of tidal formations existing in the core, each of which shows a shoaling pattern. This indicates the progradation of the delta and the influence of frequent sea level change on the depositions. It is also important to mention that the erosion events occurred in this interval, and thus started to induce the hiatus in the sedimentary history. The fluvial/delta plain phase deposition consists of fine to medium sand with occasional clay and coarse sand, which is resulted from further progradation of the delta. A lot of organic-rich layers have found in this interval. Together with the marine productivity proxies in geochemical data, it indicates a less steady fluvial environment, which still experienced marine transgression. All these sedimentary environment changes confirm the general insights from previous studies on the delta progradation in this area during the Early Pleistocene.

Provenance of the sediments has been studied by heavy mineral analysis and geochemical analysis. The results show the sediments of the core are mostly sourced from Eridanos river system, and the provenance did not change significantly to another source (e.g. Rhine-Meuse river system). This also confirms the estimated spheres of influence of different fluvial systems during the delta progradation in the southern North Sea Basin in the Pleistocene, where the Petten Borehole 1 was located mostly within or at the edge of the Eridanos catchment. However, also because of the poor recovery condition in the upper part, we cannot say for sure that there was no Rhine-Meuse influence at all in the late Early Pleistocene.

The marine/pro-deltaic phase (384 – 332 m) is the interval relatively most-continuous sedimentation, while marked erosional contacts and non-recovery intervals occur more frequently above 332 m. Also, erosion events and non-recovery complications increase towards the top of the studied section. The erosion events induced the hiatus in the sedimentary history, and thus we would lose sedimentary information. In the littoral/delta front environment, the erosions were due to frequent sea level change, and the edge of the delta is sensitive to eustasy. In the fluvial/delta plain environment, the erosions were due to river runoff (including open field erosions) and occasional transgression/regression of the sea. However, it is very difficult to find out the contacts in the core that are responsible for large-scale erosion events, because the very poor recovery condition from 220 m upwards. Also, the single lithology (massive sand) in the fluvial phase makes the searching for sedimentary hiatus harder.

References

Berendsen, H. J., & Stouthamer, E. (2000). Late Weichselian and Holocene palaeogeography of the Rhine–Meuse delta, the Netherlands. *Palaeogeography, Palaeoclimatology, Palaeoecology*, *161*(3-4), 311-335.

Busschers, F. S., Kasse, C., Van Balen, R. T., Vandenberghe, J., Cohen, K. M., Weerts, H. J. T., ... & Bunnik, F. P. M. (2007). Late Pleistocene evolution of the Rhine-Meuse system in the southern North Sea basin: imprints of climate change, sea-level oscillation and glacio-isostacy. *Quaternary Science Reviews*, *26*(25-28), 3216-3248.

Busschers, F. S., Van Balen, R. T., Cohen, K. M., Kasse, C., Weerts, H. J., Wallinga, J., & Bunnik, F. P. (2008). Response of the Rhine–Meuse fluvial system to Saalian ice‐sheet dynamics. *Boreas*, *37*(3), 377-398.

Cohen, K. M., Gibbard, P. L., & Weerts, H. J. T. (2014). North Sea palaeogeographical reconstructions for the last 1 Ma. *Netherlands Journal of Geosciences*, *93*(1-2), 7-29.

De Haas, T., Pierik, H. J., Van der Spek, A. J. F., Cohen, K. M., Van Maanen, B., & Kleinhans, M. G. (2018). Holocene evolution of tidal systems in The Netherlands: Effects of rivers, coastal boundary conditions, eco-engineering species, inherited relief and human interference. *Earth-Science Reviews*, *177*, 139-163.

Donders, T. H., Van Helmond, N. A., Verreussel, R., Munsterman, D., ten Veen, J., Speijer, R., ... & Sinninghe-Damste, J. S. (2018). Land-sea coupling of early Pleistocene glacial cycles in the southern North Sea exhibit dominant Northern Hemisphere forcing. *Climate of the Past*, *14*(3), 397-411.

Funnell, B. M. (1996). Plio-Pleistocene palaeogeography of the southern North Sea basin (3.75-0.60 Ma). *Quaternary Science Reviews*, *15*(5-6), 391-405.

Glennie, K. W., & Underhill, J. R. (1998). Origin, development and evolution of structural styles. *Petroleum geology of the North Sea: Basic concepts and recent advances*, 42-84.

Gibbard, P. L. (1988). The history of the great northwest European rivers during the past three million years. *Philosophical Transactions of the Royal Society of London. B, Biological Sciences*, *318*(1191), 559-602.

Gooday, A. J. (2002). Encyclopedia of Ocean Sciences: Benthic Foraminifera.

Haug, G. H., Hughen, K. A., Sigman, D. M., Peterson, L. C., & Röhl, U. (2001). Southward migration of the intertropical convergence zone through the Holocene. *Science*, *293*(5533), 1304-1308.

Head, M. J., & Gibbard, P. L. (2005). Early-Middle Pleistocene transitions: an overview and recommendation for the defining boundary. *Geological Society, London, Special Publications*, *247*(1), 1-18.

Head, M. J., & Gibbard, P. L. (2015). Early–Middle Pleistocene transitions: linking terrestrial and marine realms. *Quaternary International*, *389*, 7-46.

Hijma, M. P., Cohen, K. M., Roebroeks, W., Westerhoff, W. E., & Busschers, F. S. (2012). Pleistocene Rhine–Thames landscapes: geological background for hominin occupation of the southern North Sea region. *Journal of Quaternary Science*, *27*(1), 17-39.

Hodell, D. A., Channell, J. E., Curtis, J. H., Romero, O. E., & Röhl, U. (2008). Onset of “Hudson Strait” Heinrich events in the eastern North Atlantic at the end of the middle Pleistocene transition (~ 640 ka)?. *Paleoceanography*, *23*(4).

Horowitz, A. J. (1991). *A primer on sediment-trace element chemistry* (Vol. 2). Chelsea: Lewis Publishers.

Huuse, M., Lykke-Andersen, H., & Michelsen, O. (2001). Cenozoic evolution of the eastern Danish North Sea. *Marine Geology*, *177*(3-4), 243-269.

Kooi, H., Hettema, M., & Cloetingh, S. (1991). Lithospheric dynamics and the rapid Pliocene-Quaternary subsidence phase in the southern North Sea basin. *Tectonophysics*, *192*(3-4), 245-259.

Kooi, H., Johnston, P., Lambeck, K., Smither, C., & Molendijk, R. (1998). Geological causes of recent (~ 100 yr) vertical land movement in the Netherlands. *Tectonophysics*, *299*(4), 297-316.

Kuhlmann, G., de Boer, P. L., Pedersen, R. B., & Wong, T. E. (2004). Provenance of Pliocene sediments and paleoenvironmental changes in the southern North Sea region using Samarium–Neodymium (Sm/Nd) provenance ages and clay mineralogy. *Sedimentary Geology*, *171*(1-4), 205-226.

Lisiecki, L. E., & Raymo, M. E. (2005). A Pliocene‐Pleistocene stack of 57 globally distributed benthic δ18O records. *Paleoceanography*, *20*(1).

Lisiecki, L. E., & Raymo, M. E. (2007). Plio–Pleistocene climate evolution: trends and transitions in glacial cycle dynamics. *Quaternary Science Reviews*, *26*(1-2), 56-69.

López, G. I. (2017). Grain size analysis. *Encyclopedia of Geoarchaeology [Internet]. Dordrecht: Springer Netherlands*, 341-348.

Noorbergen, L. J., Lourens, L. J., Munsterman, D. K., & Verreussel, R. M. C. H. (2015). Stable isotope stratigraphy of the early Quaternary of borehole Noordwijk, southern North Sea. *Quaternary International*, *386*, 148-157.

Overeem, I., Weltje, G. J., Bishop‐Kay, C., & Kroonenberg, S. B. (2001). The Late Cenozoic Eridanos delta system in the Southern North Sea Basin: a climate signal in sediment supply?. *Basin Research*, *13*(3), 293-312.

Peterson, L. C., Haug, G. H., Hughen, K. A., & Röhl, U. (2000). Rapid changes in the hydrologic cycle of the tropical Atlantic during the last glacial. *Science*, *290*(5498), 1947-1951.

Richter, T. O., Van der Gaast, S., Koster, B., Vaars, A., Gieles, R., de Stigter, H. C., ... & van Weering, T. C. (2006). The Avaatech XRF Core Scanner: technical description and applications to NE Atlantic sediments. *Geological Society, London, Special Publications*, *267*(1), 39-50.

Rijsdijk, K. F., Passchier, S., Weerts, H. J. T., Laban, C., Van Leeuwen, R. J. W., & Ebbing, J. H. J. (2005). Revised Upper Cenozoic stratigraphy of the Dutch sector of the North Sea Basin: towards an integrated lithostratigraphic, seismostratigraphic and allostratigraphic approach. *Netherlands Journal of Geosciences*, *84*(2), 129-146.

Rothwell, R. G. (2015). Twenty years of XRF core scanning marine sediments: what do geochemical proxies tell us?. In *Micro-XRF Studies of Sediment Cores* (pp. 25-102). Springer, Dordrecht.

Ruddiman, W. F. (2014). Earth's Climate: Past and Future, Third Edition.

Schüttenhelm, R. T., & Laban, C. (2005). Heavy minerals, provenance and large scale dynamics of seabed sands in the Southern North Sea: Baak's (1936) heavy mineral study revisited. *Quaternary International*, *133*, 179-193.

Sluijs, A., Schouten, S., Donders, T. H., Schoon, P. L., Röhl, U., Reichart, G. J., ... & Brinkhuis, H. (2009). Warm and wet conditions in the Arctic region during Eocene Thermal Maximum 2. *Nature Geoscience*, *2*(11), 777-780.

van Os, B. J., Middelburg, J. J., & de Lange, G. J. (1991). Possible diagenetic mobilization of barium in sapropelic sediment from the eastern Mediterranean. *Marine Geology*, *100*(1-4), 125-136.

Westerhoff, W. E. (2009). Stratigraphy and sedimentary evolution: the lower Rhine-Meuse system during the Late Pliocene and Early Pleistocene (southern North Sea basin).

Westerhoff, W. E., Donders, T. H., Alexandre, N. T., & Busschers, F. S. (2020). Early Pleistocene Tiglian sites in The Netherlands: a revised view on the significance for Quaternary stratigraphy. *Quaternary Science Reviews*, *242*, 106417.

Zagwijn, W. H. (1985). An outline of the Quaternary stratigraphy of the Netherlands. *Geologie en Mijnbouw*, *64*(1), 17-24.

Zagwijn, W. H. (1986). The Pleistocene of the Netherlands with special reference to glaciation and terrace formation. *Quaternary science reviews*, *5*, 341-345.

Zagwijn, W. H. (1998). Borders and boundaries: a century of stratigraphical research in the Tegelen-Reuver area of Limburg (The Netherlands). *Mededelingen Nederlands Instituut voor Toegepaste Geowetenschappen TNO*, *60*, 19-34.

Ziegler, M., Lourens, L. J., Tuenter, E., & Reichart, G. J. (2009). Anomalously high Arabian Sea productivity conditions during MIS 13. *Orbital forcing of the late Pleistocene boreal summer monsoon: Links to North Atlantic cold events and El Niño–Southern Oscillation*, 71.

Appendix 1. Pictures of Interesting Observations in the Core

Fig. 1.1 *382.9 m. Bioturbation.*

Fig. 1.2 *375.4 m. Presumed bioturbation.*

Fig. 1.3 *375.25 m. Shell debris.*

Fig. 1.4 *353.3 m. Organic-rich layer.*

Fig. 1.5 *343.1 m. Black organic-rich layer.*

Fig. 1.6 *336.45 m. Non-horizontal organic-rich layers.*

Fig. 1.7 *330.25 m. Destructive structure, thought to be bioturbation.*

Fig. 1.8 *324.45 m. Shell fragments.*

Fig. 1.9 *313.27 m. Clear thin alternations of clay and sand, thought to be typical tidal formation.*

Fig. 1.10 *292.8 m. Non-horizontal structure.*

Fig. 1.11 *282.25 m. Thought to be bioturbation.*

Fig. 1.12 *237.9 m. Fine gravels.*

Fig. 1.13 *236.55 m. Rock fragments.*

Fig. 1.14 *222.23 m. Very thin alternations of clay and sand, could be tidal formation.*

Appendix 2. Potential Contacts of Hiatus

Fig. 2.1 *Contact at 314.5 m, in littoral/deltaic environment.*

Fig. 2.2 *Contact at 302.7 m, in littoral/deltaic environment.*

Fig. 2.3 *Contact at 293.05 m, in littoral/deltaic environment.*

Fig. 2.4 *Contact at 282.7 m, in littoral/deltaic environment.*

Fig. 2.5 *Abrupt lithology changes in the interval 228 – 220 m, in fluvial environment. Some changes are more abrupt, leaving a clear contact, while the others are more gradual.*

Fig. 2.6 *Contact at 216.9 m, in fluvial environment.*

Fig. 2.7 *Unrecovered interval (267.45 – 264.6 m, shown in the black box) and its sedimentary context.*